Title: Cortical granularity shapes information flow to the amygdala and its striatal targets in nonhuman primate

Abbreviated Title: Cortical granularity shapes information flow

McHale, AC[1]; Cho, YT[3], *Fudge, JL[1, 2]
University of Rochester, School of Medicine and Dentistry, Departments of Neuroscience[1] and Psychiatry[2], Rochester NY 14642; Yale University, Child Study Center and Department of Psychiatry, New Haven CT 06511[3]

*Correspondence to:
Julie L. Fudge, M.D.
Departments of Neuroscience, and Psychiatry
The Del Monte Institute for Neuroscience
University of Rochester Medical Center
julie_fudge@urmc.rochester.edu

Number of pages: 44
Number of figures: 13 (including 2 “extended data” figures)
Number of tables: 1
Number of words for abstract: 250 words
Number of words for introduction: 642 words
Number of words for discussion: 1470 words
Conflict of interest statement: The authors declare no competing financial interests.
Acknowledgements: This work was funded through the support of the National Institutes of Mental Health R01MH63291 (J.L.F.), and the Schmitt Program on Integrative Neuroscience (SPIN) GR504304 (J.L.F.). We thank Nanette Alcock for assistance with histology and immunocytochemistry. We also thank Keshov Sharma for R code advice and helpful discussions about data analysis.

Abstract

The prefrontal cortex (PFC) and insula, amygdala, and striatum form interconnected networks that drive motivated behaviors. We previously found a connectional trend in which granularity of the ventromedial and orbital PFC/insula predicted connections to the amygdala and also the scope of amygdalo-striatal efferents, including projections beyond the 'classic' ventral striatum. To further interrogate this triad and define the 'limbic (amygdala-recipient) striatum', we conducted tract tracing studies in two cohorts of primates to define the scope of cortico-amygdalo-striatal (indirect) and cortico-'limbic' striatal (direct) paths originating in the entire PFC and insula. With larger data sets and a quantitative approach, we found that the level of cortical granularity predicts the complexity and location of projections to both the amygdala and striatum. Remarkably, 'cortical-like' basal nucleus subdivisions also followed these rules in their projections to the striatum. In both 'direct' and 'indirect' paths to the 'limbic' striatum, agranular cortices formed a 'foundational', broad projection, and were joined by inputs from progressively more differentiated cortices. In amygdalo-striatal paths, the ventral basal nucleus was the 'foundational' input, with progressively more dorsal basal nucleus regions gradually adding inputs as the 'limbic striatum' extended caudally. Together, the 'indirect' and 'direct' paths follow consistent rules dictating projection strength and complexity to their targets. In the 'indirect' path, the agranular 'interoceptive' cortices consistently dominate amygdala inputs to the striatum. In contrast, 'direct' cortical inputs to the 'limbic' (amygdala-recipient) striatum create gradual shifts in connectivity fingerprints to provide clues to functional differences in the classic versus caudal ventral 'limbic' striatum.

Significance Statement

The 'limbic system' broadly refers to brain circuits that coordinate emotional responses. Here, we investigate circuits of the amygdala, which is involved in coding the emotional value of external cues, and their influence on the striatum. Regions of prefrontal cortex and insula form gradients of overlapping inputs to basal nucleus of the amygdala, which are fed forward to the striatum. Direct cortical inputs to these 'amygdala-recipient' striatal areas are surprisingly organized according to similar principles, but subtly shift from the classic ventral striatum to the caudal ventral striatum. Together, these distinct subsystems—cortico-amygdala-striatal circuits and direct cortico-striatal circuits—provide substantial opportunity for different levels of internal, sensory, and external experiences to be integrated within the striatum, a major motor-behavioral interface.

Introduction

The prefrontal cortex (PFC) and insula, amygdala, and striatum form interconnected networks that drive motivated behaviors (Van Hoesen et al., 1981; Yeterian et al., 2012). Specific cortical regions project to the amygdala, modulating amygdala neural responses (Klavir et al., 2013; Likhtik et al., 2014). At the same time, these cortical regions and the amygdala form uni-directional inputs to the striatum to mediate goal-directed responses (Haber and Knutson, 2010). This 'triadic' circuitry is implicated in human neuropsychiatric diseases (Akil et al., 2018; Ressler, 2020). Yet, organizational principles of this classic 'limbic' triad are still not completely understood at the cellular level in nonhuman primate brain.

Although they are separate lobes of cortex, the PFC and insula share a progressive change in cortical laminar differentiation (Mesulam and Mufson, 1982; Barbas and Pandya, 1989). The degree of 'granularity' across the cortical mantle generally refers to the relative presence or absence of 'granular cell' layer IV (Brodmann, 1909; Carmichael and Price, 1994; Petrides and Pandya, 1999, 2002). "Agranular" cortex lacks a granular layer IV, "dysgranular" cortex has an incompletely developed layer IV, and "granular" cortex has a well-differentiated layer IV. Within these broad categories, incremental changes in laminar organization exists, leading to gradual shifts from agranular to dysgranular to granular across the cortical mantle. Classic subdivisions of the PFC and the insula are therefore not independent regions, but rather reflect this continuous laminar organization (Barbas and Garcia-Cabezas, 2016).

The basal nucleus of the amygdala is a key recipient of top-down inputs from the PFC and insula, and is a major output to the striatum (Carmichael and Price, 1995; Ghashghaei and Barbas, 2002; Cho et al., 2013). This nucleus is expanded in primates (Stephan et al., 1987), and has an increased cytoarchitectural complexity along its dorsal-ventral axis. In monkey and human, three large subdivisions of the basal nucleus are recognized: the magnocellular (Bmc), intermediate (Bi,) and parvicellular (Bpc). As their names imply, these dorsally-to-ventrally arranged basal nucleus subdivisions are distinguished by pyramidal cell size and packing density (Braak and Braak, 1983).

Amygdala inputs are a defining input to the 'classic' ventral striatum, which is involved in forming goal-directed behaviors (Robbins et al., 1989; Popescu et al., 2009). Prior work however has demonstrated amygdala projections extend past the 'classic' ventral striatum into caudal aspects of the striatum, which we term the ‘caudal ventral striatum’ (Russchen et al., 1985; Fudge et al., 2002; Cho et al., 2013).

In a previous study, examining ‘cortico-amygdalo-striatal’ paths limited to the ventromedial and orbital PFC and insula, we found evidence that relatively higher levels of laminar organization in cortico-amygdala projections governed the topography of cortico-amygdala paths, and was also related to the extent of projections in the next limb of the circuit, the amygdalo-striatal path (Cho et al., 2013). Findings from this study raised subsequent questions around whether the most differentiated dorso-lateral regions of the PFC and insula followed this topography of inputs, and how the topography of cortico-

amygdala-striatal circuits compared to the topography of direct cortico-striatal circuits in striatal regions receiving amygdala input.

Here, we took a systems-based approach to quantitatively compare the organization of 'indirect' cortico-amygdala-striatal circuits and 'direct' cortico-striatal circuits in striatal regions receiving amygdala inputs. We first examined the entire extent of the 'indirect' path, using multiple small injection sites of bi-directional tracer focused on the specific basal nucleus subregions. In the second set of experiments, we placed small injections of retrograde tracer into territories of ‘limbic’ (amygdalo-recipient) striatum defined by the first cohort, and compared whether direct cortical-‘limbic’ striatal paths followed similar connectivity principles as indirect paths. Remarkably, we found that a recursive set of hierarchically organized connections, governed by cortical granularity, dictate both the direct and indirect cortical paths to the ‘limbic’ striatum. This organization resulted in unique connectional 'fingerprints' in subregions of the basal nucleus of the amygdala and the 'limbic' (amygdala-recipient) striatum, suggesting functional differences.

Materials and Methods

Study design. Two cohorts of *Macaca fascicularis* were used for this study (Labs of Virginia, Three Springs Laboratories, and Worldwide Primates) (Fig. 1). In the first cohort (Cohort 1), a bidirectional tracer injection was placed in various subdivisions of the basal nucleus of the amygdala. Portions of these data were previously published (Cho et al., 2013). To examine the cortico-amygdalo-striatal circuit, we charted and analyzed the number of retrogradely labeled cells in the PFC/insula, and the distribution of

134 anterogradely labeled fiber terminals in the striatum. In the second cohort (Cohort 2), we
135 used anterograde tracing maps from Cohort 1 as a guide for placing retrograde tracer
136 injections into the 'limbic' striatum (defined as striatal regions receiving amygdala input).
137 Retrogradely labeled cells in the PFC/insula and in the amygdala were then charted,
138 quantified, and analyzed.
139
140 *Surgical procedures and tissue preparation.* All surgeries were approved by the University
141 of Rochester Committee on Animal Research and follow the National Institutes of Health
142 guidelines. To conserve animals, Cohort 1 data includes new analyses in some previously
143 mapped cases (Fudge et al., 2004; Fudge et al., 2005; Cho et al., 2013; Decampo and
144 Fudge, 2013), as well as new cases. A total of 13 animals weighing between 3.3 kg and
145 9.3 kg were used across both studies (Male n = 12; Female n = 1). To determine surgical
146 coordinates, some animals had an individualized MRI T2 scan prior to surgery; others
147 had intra-operative electrophysiologic mapping (Fudge et al., 2004; Fudge et al., 2005;
148 Cho et al., 2013; Decampo and Fudge, 2013).
149
150 Monkeys that underwent individualized MRI T2 scans were first administered an
151 intramuscular injection of ketamine (10 mg/kg), then intubated with isofluorane gas during
152 the scanning process. Three days prior to stereotactic surgery, the animals received daily
153 prophylactic pain control with gabapentin (oral dose), which was maintained for 3 days
154 post-operatively. On the day of surgery, monkeys were administered an intramuscular
155 injection of ketamine (10 mg/kg), intubated, and then administered either intravenous
156 pentobarbital (initial dose, 20 mg/kg, i.v.) (animals undergoing electrophysiologic

157 mapping) or isofluorane gas anesthesia. Once monkeys were placed in a stereotactic
158 head frame, a craniotomy was performed under sterile conditions. For some animals,
159 electrophysiological mapping was conducted first, and electrophysiological features of
160 cells were noted during several penetrations. Injection sites were then plotted for
161 subsequent tracer injections.
162
163 For Cohort 1, the basal nucleus was pressure-injected at various dorsoventral and
164 rostrocaudal sites with either 40 nl of the bidirectional tracers Lucifer yellow conjugated
165 to dextran amine (LY; Invitrogen), Fluorescein conjugated to dextran amine (FS;
166 Invitrogen), or Fluoro-Ruby (tetramethylrhodamine) conjugated to dextran amine (FR;
167 Invitrogen). Antibodies to these tracers do not cross-react, and have similar retrograde
168 and anterograde properties, making them suitable for simultaneous use within the same
169 animal, based on our previous work (Haber et al., 2000; Fudge et al., 2002). For Cohort
170 2, one striatal site per animal was pressure-injected with 40 nl of wheat germ agglutinin
171 conjugated to horseradish peroxidase (WGA-HRP; Sigma). Following all surgeries, the
172 bone flap was replaced and the overlying tissue sutured. For both cohorts, animals were
173 deeply anesthetized and sacrificed via intracardiac perfusion 10 to 12 days after surgery
174 [0.9% saline solution containing 0.5 ml of heparin sulfate followed by cold 4%
175 paraformaldehyde in 0.1M phosphate buffer (PB (0.1M PO_4 pH 7.2)) and 30% sucrose
176 solution for 1 hr)]. After overnight postfixation, brains were cryoprotected in increasing
177 concentrations of sucrose solution (10%, 20%, and 30%). Brains were sectioned
178 coronally on a freezing, sliding microtome at 40 μm, placed in 24 consecutive
179 compartments containing cold cryoprotectant solution (30% sucrose and 30% ethylene

180 glycol in PB), then stored at -20°C (Rosene et al., 1986).

181

182 *Histology*

183 *Immunohistochemistry (ICC).* In both Cohorts, every eighth section through the entire
184 brain was processed using ICC for the relevant tracer. In Cohort 1, adjacent sections
185 through the striatum were processed for calbindin-D28k protein (CaBP) in order to
186 localize the position of anterogradely labeled fibers in striatal subregions (see *Amygdalo-*
187 *striatal path* section in *Cortico-amygdalo-striatal analyses*; **Cohort 1**). In Cohort 2, CaBP-
188 immunoreactivity (IR) in adjacent sections was used to localize tracer injections within
189 striatal subregions (see *Amygdalo-striatal path;* **Cohort 2**). For all experiments, tissue
190 was rinsed in phosphate buffer with 0.3% Triton-X (PB-TX) overnight. The next day, brain
191 slices were treated with an endogenous peroxidase inhibitor for 5 minutes, and then
192 underwent more rinses in PB-TX. Sections were then pre-incubated for 30 minutes in
193 10% normal goat serum blocking solution with PB-TX (NGS-PB-TX). All sections were
194 then incubated in primary antisera to LY (1:2000; Invitrogen, rabbit), FS (1:2000;
195 Invitrogen, rabbit), FR (1:1000; Invitrogen, rabbit), WGA (1:2500-1:7500 depending on
196 dilution curve; Sigma, rabbit), or CaBP (1:10,000; Millipore Bioscience Research
197 Reagents, mouse) at 4°C for four nights. Sections were then thoroughly rinsed, again
198 blocked with 10% NGS-PB-TX, and incubated for 40 minutes in the appropriate
199 biotinylated secondary antibody. After more rinses, sections with bound anti-LY, anti-FR,
200 anti-FS, anti-WGA, or anti-CaBP antibodies were incubated in an avidin-biotin complex
201 (Vectastain ABC kit; Vector Laboratories), and visualized with 3,3'- Diaminobenzidine
202 (DAB), activated with 0.3% hydrogen peroxide (H_2O_2).

203

204 *Cresyl Violet.* In order to localize cortical cytoarchitectonic boundaries for each animal
205 (both Cohorts 1 and 2), we stained 1:24 adjacent or near-adjacent sections for each case
206 with cresyl violet (Chroma-Gesellschaft, West Germany).

207

208 *Acetylcholinesterase (AChE).* In Cohort 1, AChE staining in adjacent sections was used
209 to identify injection site location in the basal nucleus, while in Cohort 2, AChE staining
210 was used to localize tracer-labeled neurons in specific basal nucleus subdivisions. For
211 both, we stained 1:24 adjacent or near-adjacent sections for AChE, using the Geneser-
212 Jensen technique (Geneser-Jensen and Blackstad, 1971).

213

214 <u>*Analysis:*</u>

215 *Cytoarchitectural criteria for the PFC and insula (Fig. 2)*

216 The PFC is defined as the frontal lobe anterior to the arcuate sulcus. Within the PFC, we
217 define the ventromedial and orbital subdivisions according to the nomenclature of
218 Carmichael and Price (Carmichael and Price, 1994), and the dorsomedial (dmPFC) and
219 dorsolateral (dlPFC) and ventrolateral (vlPFC) subdivisions according to Petrides et al.
220 (Petrides and Pandya, 1999, 2002). Insula subdivisions were defined according to
221 Carmichael and Price (Carmichael and Price, 1994). Regardless of nomenclature, all
222 cytoarchitectural maps of the PFC recognize the gradual transition from agranular to
223 granular laminar organization in the basoventral and mediodorsal direction, based on
224 laminar complexity and the relative development of layer IV (Brodmann, 1909; Preuss
225 and Goldman-Rakic, 1991; Barbas, 2007; Nieuwenhuys et al., 2007). The insula similarly

226 progresses from agranular to granular, but in a rostroventral to caudodorsal direction
227 (Mesulam and Mufson, 1982). See Supplemental Methods for detailed descriptions of
228 laminar characteristics of Brodmann's areas.
229
230 *Categorization of cortical regions by architecture*
231 For quantitative analysis, we categorized cortical areas into either 3 (general) or 9
232 (refined) categories of cortical hierarchy, based on examining layer IV thickness (for 3
233 category granularity) and the extent of layer V sublamination (for 9 category granularity)
234 under Nissl stain (Carmichael and Price, 1994) (Table 1). For 3 category granularity,
235 cortical regions were categorized as agranular cortex if they did not have layer IV,
236 dysgranular if they had incompletely developed layer IV, and granular if they had
237 completely developed layer IV.
238
239 ***Cohort 1.***
240 *Injection site placement.* Relative injection site placement within the Bmc, Bi, and Bpc
241 was determined using adjacent AChE sections for each animal. Throughout the
242 rostrocaudal extent of the basal nucleus, the Bmc is darkly stained with AChE, the Bi has
243 intermediate AChE staining, and the Bpc is lightly stained with AChE, corresponding to
244 the cytoarchitectural gradients in the nucleus (Amaral and Bassett, 1989). All nuclei, and
245 specifically basal nucleus subdivisions, were traced along with landmarks, such as blood
246 vessels across sections, and aligned over tracer-labeled sections in Adobe Illustrator
247 Creative Suite (CS).
248

249 Cases with tracer leakage into overlying structures or white matter tracts were not
250 included in the analysis. To confirm our assessment of injection site placement, we also
251 examined the pattern of retrograde labeling in brain regions known to be a source of
252 afferents to each subdivision. For example, the Bmc receives inputs from the
253 inferotemporal cortex (Herzog and Van Hoesen, 1976), while the Bpc does not; the Bpc
254 receives inputs from the hippocampus in contrast to the Bi and Bmc (Saunders et al.,
255 1988; Fudge et al., 2012).
256
257 *Cortico-amygdalo-striatal analyses*
258 *Cortico-amygdala path.* Retrogradely labeled cells in 1:24 sections were charted through
259 the entire rostral-caudal extent of the PFC and insula using an Olympus AX70 microscope
260 interfaced with Neurolucida, via a video CCD (Microbrightfield, Williston, VT).
261 Cytoarchitectural boundaries of cortex using traditional nomenclature were determined
262 on adjacent Cresyl violet-stained sections under the microscope. These labeled charts
263 were then aligned onto maps of retrogradely labeled cells in Adobe Illustrator CS. The
264 number of retrogradely labeled cells in each cortical subdivision was counted using the
265 Adobe Illustrator "objects" count feature. Cortical regions for each region were then
266 categorized into 3- and 9-category "agranular", "dysgranular", and "granular" groupings
267 as described above (Table 1).
268
269 After assignment of each cortical area to a cortical granularity category, we used the
270 "*circlize"* package in R (R Foundation for Statistical Computing, Vienna, Austria) to
271 generate chord diagrams of our retrograde cortical data, using our 3 and 9 category

classifications of cortical granularity (Gu et al., 2014). Chord diagrams are an effective way to visualize the directionality and connectivity between different nodes of a data set. 'Fragments', which represent each node, are found along the outer perimeter of the plot. Color-coded chords display the directionality and strength of connections between 'fragments'. If the color of a chord and a 'fragment' are the same, this indicates how that 'fragment' is connected to other nodes in the data set (i.e. how the agranular cortex 'fragment' projects into various basal nucleus injection site 'fragments'). Chord thickness indicates the relative strength or weakness of connections between nodes (i.e. chord thickness represents the number of retrogradely labeled cells originating from a granularity 'fragment'). The small tic marks and numbers found along the axis of each 'fragment' indicate number of cells.

Amygdalo-striatal path. Anterogradely labeled terminal fibers were hand-charted through the rostro-caudal extent of the striatum with the aid of a drawing tube under dark-field illumination. Labeled thick fibers that did not contain boutons were considered fibers of passage and were therefore not included. All hand-drawn charts were then scanned at high resolution and converted in Adobe Illustrator CS for formatting. Striatal boundaries were then determined through comparison to adjacent or near-adjacent CaBP-labeled sections. CaBP-labeled sections were projected onto paper maps of anterogradely labeled fibers in the striatum. Landmarks including blood vessels and fiber tracts were carefully aligned, and CaBP-positive and CaBP-negative areas of the striatum were drawn in. Maps were then scanned into digital format at high resolution, and converted in Adobe Illustrator CS.

295

296 ***Cohort 2.***

297 *Injection site placement.* Injection sites were targeted to the rostral ventral striatum, and
298 also to regions of the ventromedial striatum posterior to the anterior commissure, based
299 on anterograde maps from Cohort 1. Injection site position was determined with
300 reference to adjacent CaBP-labeled sections. CaBP-poor regions were used to identify
301 the 'shell' (Meredith et al., 1993; Fudge and Haber, 2002). All injection sites that resulted
302 in retrogradely labeled cells in the amygdala were used for Cortico-'limbic' striatum and
303 Amygdalo-striatal analyses.

304

305 *Amygdalostriatal path.* The location and quantification of retrogradely labeled cells in
306 basal nucleus subdivisions was mapped in 1:24 sections, with reference to adjacent
307 AChE stained sections. All retrogradely labeled cells in the amygdala were subsequently
308 sorted by subdivision (Bmc, Bi, and Bpc) based on levels of AChE activity and cellular
309 features, and analyzed with respect to position of the injection within the striatum.

310

311 *Cortico-'limbic' striatal path.* Only injection sites resulting in significant numbers of labeled
312 cells in the basal nucleus (>10) were used for these analyses. We quantified retrogradely
313 labeled cells in the entire PFC and insula, and applied the same criteria for classification,
314 analysis, and visualization described for Cohort 1.

315

316 *Comparing cortico-amygdala-striatal and cortico-striatal pathways*. To first address
317 whether amygdala neuronal populations projecting to different striatal regions received a

318 similar balance of agranular, dysgranular, and granular cortical inputs, we used a 'ratio of
319 ratios' approach to examine data across Cohort 1 (cortico-amygdala) and Cohort 2
320 (amygdala-striatal). We first pooled the sum of all agranular, dysgranular, and granular
321 labeled cell counts resulting from Bmc, Bi, and Bpc injection sites (i.e. cortico-amygdala
322 data), and converted these sums into percentages. Only basal nucleus injection sites
323 that were wholly confined to one of these subdivisions were used. Once the proportion
324 of labeled neurons in the agranular, dysgranular, and granular cortex were determined
325 for Bmc, Bi, and Bpc injection groupings, we multiplied these percentage values by the
326 number of retrogradely labeled cells in Bmc, Bi, and Bpc resulting from each striatal
327 injection site in Cohort 2. We then converted this sum into a final percentage value to
328 assess the balance of agranular, dysgranular, and granular cortical inputs to amygdala-
329 striatal projecting cells for each striatal site. We finally conducted bootstrap analysis to
330 check the 'stability' of our final percentage values in 'indirect' pathway calculations. We
331 did 4 replicates of the data, and found that the average difference of full versus bootstrap
332 data was = 1.4%, the median was 1.0%, the SD was 0.01198, the maximum was 5.6%,
333 and the minimum was 0.1%. The proportion of labeled cells in the agranular, dysgranular,
334 and granular cortices for the indirect pathway (conjunction of Cohort 1 cortico-amygdala
335 data and Cohort 2 amygdalo-striatal data) were then compared to the proportion of
336 labeled cells in agranular, dysgranular, and granular cortices for each injection site
337 associated with the direct cortico-striatal pathway (Cohort 2). Results were expressed as
338 the proportion of labeled neurons in the agranular, dysgranular, and granular cortex
339 associated with each path for each striatal injection site.
340

341 **Results**

342 ***Cortico-amygdalo-striatal paths (Cohort 1)***

343 *Basal nucleus injection site placement (Fig. 3)*. In the Bmc, there were three injections
344 placed at slightly different levels—cases J12LY, J16LY, J12FR—as well as five injections
345 at different levels of the Bpc—cases J20LY, J15LY, and J14FR in rostral Bpc, and cases
346 J15FS and J14FS in caudal Bpc, all reported previously (Cho et al., 2013). Three new
347 injections at slightly different levels of the Bi—cases J47FS, J44FR, and J52LY were
348 made and assessed for a more complete survey of the basal nucleus subdivisions. The
349 Bi injection in J47FS was the most ventral, the injection in J52LY extended slightly more
350 dorsally, and the injection in J44FR was most dorsal and lateral, straddling the border
351 with the lateral Bmc.

352

353 *Cortical inputs along basal nucleus subdivisions (Fig. 4)*. After all injections in the basal
354 nucleus, a general pattern emerged in which injection sites placed in the Bpc resulted in
355 many labeled cells in the PFC and insula, restricted to the agranular PFC and insula,
356 while increasingly dorsal and rostral injections in the Bpc, Bi, and Bmc resulted in labeled
357 cells in broader cortical regions, as detailed below.

358

359 *Bpc.* Injection sites in the Bpc (cases J15FS, J14FS, J14FR, J20LY, J15LY) resulted in
360 labeled cells largely confined to agranular cortex, i.e. area 25c, 14c, and agranular insula
361 areas (Fig. 4A). J15FS and J15LY had the most labeled cells in agranular insula
362 subdivisions Iapm and Ial, J14FS had most labeling in Iai and Iapl, J14FR had most
363 labeling in Iapl, and J20LY had most labeling in Ial and Iapl. Across Bpc cases, the

364 majority of labeled cells was in the agranular insula rather than PFC, however, the
365 proportion of labeled cells in the agranular PFC increased gradually as the injection sites
366 were positioned more laterally. Case J15LY, which is an injection in the 'transition'
367 between the Bpc and Bi, had additional labeling in agranular area 24a. J20LY had
368 relatively more labeled cells in dysgranular insula compared to other Bpc sites.
369
370 *Bi.* Bi injections sites (cases J47FS, J52LY, and J44FR) resulted in the majority of labeled
371 cells in agranular cortices, but with a relatively greater contribution of labeled cells in
372 dysgranular and granular cortices compared to Bpc (Fig. 4A). Similar to Bpc, high
373 numbers of labeled cells were found in 25c, 14c, and agranular insula. Case J47FS had
374 the most labeled cells in Iapm and Iai, case J52LY had the majority of labeled cells in Iai
375 and Ial, and case J44FR had the most labeled cell in Iapl. In contrast to Bpc sites, a
376 broader distribution of labeled cells occupied relatively more differentiated agranular
377 areas, including 32c, 24a, 24b, and 13a, as well as labeled cells in dysgranular regions
378 such as area 13b. J44FR, located in a 'transition' region between Bi and Bmc, had
379 relatively more labeled cells in agranular area 24c, dysgranular insula, and 8B, in addition
380 to labeled cells specifically in granular areas 12l and 8Ad.
381
382 *Bmc.* While the majority of labeled cells remained in the agranular regions of PFC and
383 insula, injections in Bmc cases (J12FR, J16LY, and J12LY) had the broadest distribution
384 of labeled cells. Similar to Bpc and Bi, Bmc had many labeled cells in agranular areas
385 25c, 14c, and agranular insula. Similar to Bi cases, Bmc cases had high levels of labeled
386 cells in agranular areas 24a, 24b, and 24c, but in contrast, also had moderate numbers

387 of labeled cells in dysgranular areas 14r, 8B, 13m, and 12o, and some labeled cells in
388 granular areas 45, 9, 8Ad, 8Av, and 46.
389
390 Quantitative analyses revealed that cortical granularity subtype, rather than association
391 with the insula or PFC, predicted inputs across, and even within, basal nucleus
392 subdivisions (Fig. 4B). The agranular cortices in both PFC and insula contained labeled
393 cells after all basal nucleus injections, but were the sole contributor when injection sites
394 were placed in the caudomedial Bpc. Labeled cells in dysgranular cortices appeared and
395 increased in numbers following injections along the rostro-dorsal axis, from the rostro-
396 medial Bpc to Bi to Bmc. Labeled cells in the granular cortices of the insula and PFC
397 formed a relatively smaller contribution, seen only after injections in dorsal Bi and Bmc.
398 The pattern of inputs was nested such that labeled cells in incrementally higher levels of
399 cortical organization only appeared in conjunction with labeled cells in less differentiated
400 cortical areas. Analyses using the more refined (9 category) granularity classification
401 showed a similar, nested pattern (Fig. 4-1). In these, subcategories of differentiation
402 within a general granularity 'level' were themselves overlapping in a hierarchical manner.
403
404 ***Basal nucleus-striatal path.*** The distribution and relative density of anterogradely
405 labeled fibers in the striatum from each basal nucleus injection site were mapped (Fig. 5).
406 While all injections sites in the basal nucleus subdivisions resulted in labeled fibers in the
407 shell of the nucleus accumbens, the distribution of labeled fibers varied predictably,
408 expanding its distribution in the striatum as injection site position moved from the
409 caudomedial to rostro-dorsal basal nucleus.

410

411 *Bpc.* Caudomedial Bpc injections (Cases J14FS, J15FS) had labeled fibers largely
412 confined to the dorsomedial shell of the ventral striatum, while more rostral and lateral
413 Bpc injections (J20LY, J14FR, J15LY) resulted in additional labeled fibers in the medial
414 and lateral shell of the ventral striatum, interstitial nucleus of the anterior commissure
415 (IPAC, or fundus striatii), and a small region of the caudomedial putamen caudal to the
416 anterior commissure.

417

418 *Bi.* Bi injection sites (cases J47FS, J52LY, and J44FR) resulted in labeled fibers in the
419 same regions as Bpc inputs, except for the dorsomedial shell (Fig. 5). Compared to Bpc
420 cases, Bi injection sites had additional light distributions of labeled fibers in the central
421 rostral 'core' of the ventral striatum, and moderate to heavy labeled fibers in the ventral
422 body of the caudate nucleus, amygdalostriatal area, ventral putamen posterior to the
423 anterior commissure, and tail of the caudate nucleus. Anterogradely labeled fibers
424 continued caudally to fill the genu of the caudate nucleus.

425

426 *Bmc.* The broad pattern of labeled fibers (cases J12FR, J16LY, and J12LY) resembled
427 those in the Bi, including high densities of labeled fibers in the ventral body of the caudate
428 nucleus, amygdalostriatal area, ventral putamen posterior to the anterior commissure,
429 and tail of the caudate nucleus. Labeled fibers in the rostral ventral striatum were mainly
430 found in the lateral shell, and Bmc injections had more labeled fibers in central domains
431 of the caudate head compared with Bi injections.

432

433 ***Cortico-striatal and amygdalo-striatal paths (Cohort 2)***

434 *Injection site placement*. 8 injections were placed into a range of rostral-caudal striatal
435 regions that received amygdala input based on Cohort 1 anterograde data (Fig. 6). Of
436 these, 6 sites had large numbers of retrogradely labeled cells in the basal nucleus, and
437 were used for analysis. Of these, 2 injections are located in the rostral ventral striatum;
438 J24WGA was placed in the CABP-negative dorsomedial shell, and J13WGA was placed
439 in the CaBP-positive ventral striatal core. 4 injections are located in more caudal ventral
440 striatal regions; J8WGA, J12WGA, and J11WGA were all placed at different levels of the
441 caudoventral putamen. J41WGA was placed in the ventromedial body of the caudate
442 nucleus posterior to the anterior commissure. 2 injections had relatively few labeled cells,
443 and were not included in the analysis (J35FR and J42WGA).

444

445 ***Amygdala inputs delineate 'limbic' striatum regions.*** The basal nucleus had many
446 labeled cells after all injections (Figs. 7A). Other amygdala nuclei, especially the
447 accessory basal nucleus (magnocellular subdivision), had labeled cells in some cases
448 (data not shown). In general, the total number of labeled cells in the basal nucleus was
449 highest following rostral ventral striatal injections, decreasing with injections in
450 progressively caudal sites (Fig 7B). With increasingly caudal injection sites, labeled cells
451 also were found in the Bi and Bmc. The pattern of inputs from the basal nucleus
452 subdivisions resembled the hierarchical layering of cortical inputs to the basal nucleus
453 found in Cohort 1. The Bpc formed ubiquitous input to all striatal regions, with additional
454 inputs sequentially added from Bi and Bmc, respectively, in increasingly caudal ventral
455 striatal regions. We termed these caudal regions 'extended' caudal ventral striatum.

456

457 ***Direct cortical inputs to 'limbic' striatum regions.*** All 6 striatal cases contained
458 labeled cells in both the PFC and insula (Fig. 8A). There were labeled cells in the
459 agranular cortex after all injection sites. The injection site in the dorsomedial shell of the
460 striatum resulted in labeled cells almost exclusively in the agranular cortices, while the
461 injection site in the ventral striatal 'core' resulted in additional labeled cells in dysgranular
462 cortices. Injections in more caudal sites of the ventral striatum led to more labeled cells
463 in dysgranular and granular cortices. Overall, the greatest number of labeled cells from
464 the PFC and insula were seen following injections into the rostral ventral striatum, with
465 numbers tapering off following injections in more 'caudal limbic striatum'.

466

467 *'Classic' ventral striatum.* Agranular cortices had many labeled cells in cases J24WGA
468 and J13WGA, particularly areas 25c, 25r, 32c, 32r, and agranular insula (Fig. 8A). Both
469 J24WGA and J13WGA had many labeled cells specifically in areas 25 and Iai, but
470 J13WGA, placed in the ventral striatal core, had many additional labeled cells in Ial, as
471 well as many labeled cells in agranular areas 14c and 24b, and dysgranular area 13b.

472

473 *Caudal ventral striatum.* Injections into the caudoventral putamen (J8WGA, J11WGA,
474 and J12WGA) and the ventral body of the caudate head (J41WGA) resulted in labeled
475 cells in the agranular cortices, as did our rostral ventral striatal site (Fig. 8A). The number
476 of labeled cells from agranular cortices decreased along the rostrocaudal axis overall,
477 balanced by increasingly more labeled cells appearing in the dysgranular and granular
478 cortices. For example, cases J8WGA and J12WGA had a majority of cell labeling in

479 agranular insula, but in cases J11WGA and J41WGA agranular insula labeling was more
480 modest, with relatively more labeling in dysgranular insula. Similarly, the number of
481 labeled neurons in agranular area 25 declined along the rostrocaudal axis. All caudal
482 injection sites had many labeled cells in dysgranular insula, and moderate cell labeling in
483 granular insula.
484
485 Quantitative analyses revealed hierarchical, nested projections based on basic levels of
486 cortical differentiation (Fig. 8B). This pattern was similar to that observed in cortico-
487 amygdala retrograde data, with agranular regions containing retrogradely labeled cells
488 for all injection sites, and increasingly caudal regions containing labeled cells in
489 dysgranular and granular cortices of both the insula and PFC. Analyses using a more
490 refined (9 category) granularity classification showed similar patterns (Fig. 8-1).
491
492 ***Comparing granularity index for cortico-amygdala-striatal and cortico-striatal***
493 ***pathways***. We used a 'ratio of ratios' approach to estimate how cortical granularity
494 influenced amygdala projections to specific striatal regions in the 'indirect' pathway (see
495 Methods) and compared these results with results for the direct pathway (Fig. 9). For all
496 striatal injection sites, agranular cortical sources dominated in both pathways, followed
497 by a smaller contribution from dysgranular cortices, and the smallest from granular
498 cortices (Fig. 9A). For the indirect pathway, input from each type of cortex remained
499 relatively stable across the rostro-caudal extent of striatal injection sites. In contrast, in
500 the direct pathway there was a shift in the relative contribution from agranular,
501 dysgranular, and granular cortices along the rostrocaudal axis of the amygdala-recipient

('limbic') striatum. In this path, the contribution from agranular cortical regions was progressively reduced, with increasing input from more differentiated cortices. Taken together, in the 'classic' ventral striatal regions, the balance of cortical influences is similar, whether direct, or indirectly processed through the amygdala. In more 'caudal ventral striatum', while the balance of 'indirect' cortical influence remained constant, direct inputs from the cortex varied. The agranular cortical inputs were less pronounced, but maintained a presence, along with increased dysgranular and granular cortical inputs (Fig. 9B).

<u>Cortical granularity maps: translating to traditional cortical divisions</u>

After analyzing data using cortical granularity criteria, we were interested in understanding how the combinations of traditional cortical regions comprised these patterns. It has long been known that 'agranular' cortices are associated with the 'limbic' system, while dysgranular cortices are considered 'paralimbic' and the most granulated cortices are associated with higher cognitive functions (Badre and D'Esposito, 2009; Barbas, 2015). Since functional studies are typically based on Brodmann's areas and atlas designations, we 'back-translated' the granularity index findings by converting the data according into its original atlas designation (Table 1)(Fig. 10).

In the cortico-amygdala path, the greatest contribution to the 'agranular' cortex was from agranular insula, where the numbers of labeled cells were greater than in all regions of the agranular cortex of the PFC combined (anterior cingulate areas 25, 24, and 32) (Fig 10A, blue). The agranular insula was associated with all basal nucleus subdivisions. In

525 the Bpc, agranular insula was surprisingly dominant compared to area 25, especially in
526 more caudomedial regions, based on cell count criteria. Labeled cells in area 25 resulted
527 mainly from injection sites in the rostro-dorsal Bpc as well as the ventral Bi. In a similar
528 manner, the number of labeled cells in areas 24 and 32 increased mainly from Bi and
529 Bmc injection sites, having little association with Bpc injection sites.
530
531 Contributions from dysgranular cortices were mainly from dysgranular area 13,
532 dysgranular area 8 (i.e. area 8B), dysgranular area 12 (i.e. 12o), and the dysgranular
533 insula (Fig. 10A, aqua, green). Area 13 was associated mostly with Bmc injection sites,
534 area 8 associated mostly with dorsal Bi and Bmc injection sites, area 12 associated mostly
535 with dorsal Bi and Bmc injection sites, and dysgranular insula associated with rostral Bpc,
536 dorsal Bi, and Bmc injection sites. In the granular cortices there was modest numbers of
537 labeled cells in regions of the dorsal and lateral PFC (areas 9, 46, 45) and frontal pole
538 (area 10). The granular insula (Ig) had the fewest labeled cells. All of these regions were
539 associated mainly with the dorsal Bi and Bmc.
540
541 In the cortico-striatal path, the agranular cortex as a whole had its largest contribution
542 from the agranular insula, followed by area 25. Labeled cells in the agranular insula were
543 associated with all striatal sites, while labeled cells in area 25 were associated mainly
544 with rostral ventral striatal injection sites. Areas 24 and 32 contained labeled cells in all
545 striatal injection sites, which were prominent in the rostral striatum, but persisted in
546 association with every caudal ventral striatal site. Contributions from the dysgranular
547 component of area 13 (i.e. area 13b) (aqua) and dysgranular insula (light green) were

548 first seen in the core of the rostral ventral striatum, and were present through the caudal
549 ventral striatum. The dysgranular insula (light green) was a key contributor following all
550 caudal ventral striatal injection sites. The number of labeled cells in combined
551 dysgranular/granular (orange/red) cortices was most prominent in area 12 (specifically
552 area 12o), with lesser contributions from other combined dysgranular/granular and fully
553 granular cortices. Labeled cells in all these regions were associated with the core of the
554 rostro-ventral striatum, and caudal ventral striatal sites. The 'core' of the rostral ventral
555 striatum had the most labeled cells overall, compared to other injection sites. Labeled
556 cells from the PFC and insula generally declined in 'extended' caudal ventral striatal
557 regions. These regions receive additional massive inputs from sensory association
558 cortices not examined in this study (Saint-Cyr et al., 1990; Yeterian and Pandya, 1995,
559 1998) (see Discussion).

560

561 **Discussion**

562 There were several important findings that emerged from these studies. The first is that
563 a ‘cortical logic’ governed by laminar structure shapes information flow in both the
564 ‘indirect’ and ‘direct’ paths to the 'limbic' striatum (Fig. 11). Agranular cortical inputs to
565 both the amygdala and striatum were foundational, undergirding inputs from incrementally
566 more differentiated cortex in a strict progression based on laminar assignment.
567 Remarkably, these basic organizational principles were also present in the amygdalo-
568 striatal path, which emanated from cytoarchitecturally defined subregions of the basal
569 nucleus. While not a laminar structure, the basal nucleus is cortical-like (Carlsen and
570 Heimer, 1988), and appears to follow hierarchical rules found in cortical projections.

571 Another key result was that the amygdala-striatal paths were influenced by a consistent
572 proportion of agranular/dysgranular/granular cortices, overwhelmingly dominated by
573 agranular cortex, regardless of whether the final target was the rostral-ventral or caudal-
574 ventral striatum. In contrast, the ratio of cortical laminar regions in the direct cortico-
575 amygdala projection was more changeable, and became gradually tipped to favor of more
576 differentiated inputs in the caudal ventral striatum.
577
578 Finally, we concluded that the 'limbic' striatum, as defined by amygdala inputs, extends
579 beyond the 'classic' ventral striatum (nucleus accumbens). Different rostrocaudal levels
580 of the 'limbic' striatum receive shifting combinations of cortical inputs, making for unique
581 'connectional fingerprints' in each region.
582
583 ***Cortical logic.*** Many individual studies have examined pathways linking cortex to
584 amygdala, amygdala to the striatum, and cortex to the striatum, using anterograde tracer
585 injections into the cortex (Mufson et al., 1981; Russchen et al., 1985; Goldman-Rakic and
586 Selemon, 1986; Carmichael and Price, 1995; Ferry et al., 2000; Ghashghaei and Barbas,
587 2002; Fudge et al., 2004). Our work builds on these studies by taking a 'connectomics'-
588 type approach, examining the relationship of multiple pathways within and across
589 animals, and assessing rules by which top-down cortex modulates down-stream targets.
590 This approach is based on a basic tenet that functional specificity is determined by
591 ensembles of afferent projections, and that the strength of any one connection depends
592 on features of the afferents that arrive with it.
593

The principles that guide the 'logic' of cortical afferents are based in the granular complexity of the cortical afferent source. The least differentiated cortical regions examined form a 'foundational' base across the basal nucleus and 'limbic' (amygdala-recipient) striatum, while inputs from more differentiated cortical regions are additive and are always seen as co-projections with these less differentiated cortical regions.

One way to view the broad 'foundational' influence of agranular cortices versus the relatively more restricted influence of differentiated cortices is by applying emerging ideas about differential functions of cortical afferent systems (Sherman and Guillery, 1998). This concept is based on Sherman and Guillery's 'driver-modulator' theory of excitatory afferents, in which a 'driver pathway' provides the main path of information flow and a co-projecting 'modulator pathway' regulates the output from 'driver' systems (Sherman and Guillery, 1998). Applied to our work here, we hypothesize that the agranular cortices of the PFC and insula are a driver system of both 'indirect' cortico-amygdala-striatal and 'direct' cortico-striatal circuits. These regions, along with the entirety of the basal nucleus and amygdala-recipient striatum form the foundational circuits that may be responsible for carrying salient emotional information forward. The other networks composed of dysgranular and granular cortices, the Bi, Bmc and caudal ventral striatum may function as modulator pathways—more restricted in their influence, with possible regulation of the foundational pathways with which they co-project. Specific anatomic and electrophysiologic properties define 'driver/modulator' paths, and can be tested in this system in the future.

617 ***“Connectivity Fingerprints” in the Basal nucleus and 'Limbic' Striatum***

618 Due to the ‘logic’ of cortical afferents, a predictable, yet unique set of inputs are found in
619 specific subregions of both the basal nucleus and the striatum. Unique connectivity
620 profiles ('fingerprints') are found in ventral-dorsal (basal nucleus) and rostral-caudal
621 (striatum) locations, and shift in a predictable, topographical manner.

622

623 *Basal nucleus ‘fingerprints’.* Against a backdrop of broad-based agranular cortical inputs,
624 projections from increasingly dysgranular and granular cortical regions are added, and
625 overlapped in incrementally dorsal and rostral aspects of the basal nucleus. These
626 additions to connectivity appeared to closely follow differences in its pyramidal cell size
627 along the ventral (Bpc) to dorsal (Bmc) gradient of the basal nucleus. Pyramidal neurons
628 in the dorsal (Bmc) basal nucleus, which receive the most diverse set of cortical inputs,
629 are known to be the largest in the amygdala (Amaral et al., 1992), followed by decreasing
630 cell size in the intermediate and ventral basal nucleus. Cell soma size, along with synaptic
631 contact number and channel density, governs neuronal information coding (Sengupta et
632 al., 2013). Cell soma size is the factor most associated with a high information coding
633 capacity, when synaptic numbers and channel densities are held constant. Based on
634 size alone, neurons in the Bmc thus appear best-equipped for integrating the large
635 numbers of cortical afferent inputs from overlapping limbic and cognitive cortical
636 networks, as well as coordinating efferent outputs to vast striatal regions. This supports
637 our finding that the Bmc received the most diverse set of cortical inputs and projected the
638 most diverse set of striatal outputs.

639

640 Gradual connectional shifts in the basal nucleus may also be guided by its prenatal
641 developmental patterns. Bmc neurons are the 'oldest' neurons in the basal nucleus
642 based on birth-dating studies done in the fetal macaque (Kordower et al., 1992). By
643 inference, these more dorsal basal nucleus neurons can begin the simultaneous process
644 of somal growth and differentiation and afferentation at earlier timepoints (Purves and
645 Lichtman, 1980; Dalva et al., 1994) , perhaps with time for contact by more diverse
646 cortical inputs.
647
648 *'Limbic' striatal 'fingerprints'* The classic ventral striatum (also known as the nucleus
649 accumbens) mediates reward-driven behaviors (Haber and Knutson, 2010) based in part
650 on amygdala inputs (Popescu et al., 2007; Dallerac et al., 2017). In contrast, the caudal
651 ventral striatum has long been considered important in multimodal sensory integration
652 and discrimination, based on strong inputs from visual and auditory systems (Saint-Cyr
653 et al., 1990; Yeterian and Pandya, 1995, 1998; Amita et al., 2019). Our data expand the
654 connectivity profile of the caudal ventral striatum, showing it to be part of the 'limbic'
655 striatum based on amygdala inputs. In addition to the direct agranular cortical inputs that
656 are foundational in the entire 'limbic' striatum, the caudal ventral striatum receives
657 additional inputs from the dysgranular insula, area 12, and area 8. These cortical regions
658 are involved in awareness of bodily movements, and social responses (Karnath and
659 Baier, 2010; Jezzini et al., 2012) see review (Evrard, 2019), object identification (Wilson
660 et al., 1993), and eye and ear movement (Bon and Lucchetti, 1994), respectively. Taken
661 together with caudal ventral striatal visual/auditory inputs in primate species, this
662 connectional fingerprint suggests a role in motivated multisensory responses, including

complex social interactions involved in saccades, vocalizations, and head and neck movements.

Functional network organization. Throughout the 'direct' and 'indirect' paths to the limbic striatum, an extensive foundation is created by the agranular cortex, comprised of structures involved in internal salience monitoring (Craig, 2002). This is coupled with the greater specificity in dysgranular and granular cortex connectivity (regions implicated in social interactions (Sliwa and Freiwald, 2017) and multi-modal sensory integration/the 'ventral attention network' (Fox et al., 2006), respectively). We speculate that the overlap of these latter regions in paths involving the dorsal basal nucleus and caudal ventral striatum may provide necessary structural organization by which social-emotional behavior arises in primates. The hierarchical, layered connectivity profiles, which are most expanded in these latter regions, may promote behavioral flexibility, particularly for the emotional and cognitive integration required when engaging in complex social groups (Chang et al., 2013).

This connectional complexity could leave the striatum, particularly the caudal striatum, susceptible to neuropsychiatric diseases, particularly those in which auditory/visual processing deficits interface with the limbic system. Our work shows that the caudal striatum receives more 'limbic' inputs than previously noted which presumably project onto, and along with, these strong visual and auditory circuit terminals (Saint-Cyr et al., 1990; Yeterian and Pandya, 1995, 1998). Therefore, it is possible that abnormalities in the 'connectivity fingerprint' intrinsic to the caudal striatum may be involved in perceptual

686 disturbances such as psychosis, as suggested by human neuroimaging studies (Hoffman
687 et al., 2011; Cui et al., 2016).
688
689 ***Conclusion***
690 Cortical granularity rules were elucidated in a well-known triad of connections through the
691 'limbic' brain in monkeys. Using a connectomics-type approach, we found that the basal
692 nucleus and 'limbic' striatum are not homogeneous entities, and have unique, predictable,
693 sets of 'connectivity fingerprints' within them. These general connectivity patterns have
694 implications for the ways in which the emotional brain can code increasingly complex
695 levels of social and cognitive information in a flexible manner, such as predicting actions
696 and choices of others (Saez et al., 2015; Grabenhorst et al., 2019), and may help us to
697 better understand dynamics in complex neuroanatomic circuits associated with human
698 psychiatric disease.
699
700
701
702 **Bibliography**

703 Akil H, Gordon J, Hen R, Javitch J, Mayberg H, McEwen B, Meaney MJ, Nestler EJ (2018)
704 Treatment resistant depression: A multi-scale, systems biology approach.
705 Neuroscience and biobehavioral reviews 84:272-288.
706 Amaral DG, Bassett JL (1989) Cholinergic innervation of the monkey amygdala: An
707 immunohistochemical analysis with antisera to choline acetyltransferase. J Comp
708 Neurol 281:337-361.
709 Amaral DG, Price JL, Pitkanen A, Carmichael ST (1992) Anatomical organization of the
710 primate amygdaloid complex. In: The Amygdala: Neurobiological Aspects of Emotion,
711 Memory, and Mental Dysfunction, pp 1-66: Wiley-Liss, Inc.
712 Amita H, Kim HF, Smith MK, Gopal A, Hikosaka O (2019) Neuronal connections of direct and
713 indirect pathways for stable value memory in caudal basal ganglia. The European
714 journal of neuroscience 49:712-725.

Badre D, D'Esposito M (2009) Is the rostro-caudal axis of the frontal lobe hierarchical? Nature reviews Neuroscience 10:659-669.
Barbas H (2007) Specialized elements of orbitofrontal cortex in primates. Annals of the New York Academy of Sciences 1121:10-32.
Barbas H (2015) General cortical and special prefrontal connections: principles from structure to function. Annual review of neuroscience 38:269-289.
Barbas H, Pandya DN (1989) Architecture and intrinsic connections of the prefrontal cortex in the rhesus monkey. J Comp Neurol 286:353-375.
Barbas H, Garcia-Cabezas MA (2016) How the prefrontal executive got its stripes. Curr Opin Neurobiol 40:125-134.
Bon L, Lucchetti C (1994) Ear and eye representation in the frontal cortex, area 8b, of the macaque monkey: an electrophysiological study. Exp Brain Res 102:259-271.
Braak H, Braak E (1983) Neuronal types in the basolateral amygdaloid nuclei of man. Brain research bulletin 11:349-365.
Brodmann K (1909) "Vergleichende Lokalisationslehre der Grosshirnrinde" (Comparitive Localization Theory of the Cerebral Cortex: Illustrated in its Principles on the Basis of Cell Construction). Leipzig: J.A. Barth.
Carlsen J, Heimer L (1988) The basolateral amygdaloid complex as a cortical-like structure. Brain research 441:377-380.
Carmichael ST, Price JL (1994) Architectonic subdivision of the orbital and medial prefrontal cortex in the macaque monkey. J Comp Neurol 346:366-402.
Carmichael ST, Price JL (1995) Limbic connections of the orbital and medial prefrontal cortex in macaque monkeys. J Comp Neurol 363:615-641.
Chang SW, Brent LJ, Adams GK, Klein JT, Pearson JM, Watson KK, Platt ML (2013) Neuroethology of primate social behavior. Proceedings of the National Academy of Sciences of the United States of America 110 Suppl 2:10387-10394.
Cho YT, Ernst M, Fudge JL (2013) Cortico-Amygdala-Striatal Circuits Are Organized as Hierarchical Subsystems through the Primate Amygdala. The Journal of neuroscience : the official journal of the Society for Neuroscience 33:14017-14030.
Craig AD (2002) How do you feel? Interoception: the sense of the physiological condition of the body. Nature Reviews Neuroscience 3:655-666.
Cui LB, Liu K, Li C, Wang LX, Guo F, Tian P, Wu YJ, Guo L, Liu WM, Xi YB, Wang HN, Yin H (2016) Putamen-related regional and network functional deficits in first-episode schizophrenia with auditory verbal hallucinations. Schizophr Res 173:13-22.
Dallerac G, Graupner M, Knippenberg J, Martinez RC, Tavares TF, Tallot L, El Massioui N, Verschueren A, Hohn S, Bertolus JB, Reyes A, LeDoux JE, Schafe GE, Diaz-Mataix L, Doyere V (2017) Updating temporal expectancy of an aversive event engages striatal plasticity under amygdala control. Nature communications 8:13920.
Dalva MB, Ghosh A, Shatz CJ (1994) Independent control of dendritic and axonal form in the developing lateral geniculate nucleus. The Journal of neuroscience : the official journal of the Society for Neuroscience 14:3588-3602.
Decampo DM, Fudge JL (2013) Amygdala projections to the lateral bed nucleus of the stria terminalis in the macaque: Comparison with ventral striatal afferents. The Journal of comparative neurology 521:3191-3216.
Evrard HC (2019) The Organization of the Primate Insular Cortex. Front Neuroanat 13:43.

760 Ferry AT, Ongur D, An X, Price JL (2000) Prefrontal cortical projections to the striatum in
761 macaque monkeys: evidence for an organization related to prefrontal networks.
762 Journal of Comparative Neurology 425:447-470.
763 Fox MD, Corbetta M, Snyder AZ, Vincent JL, Raichle ME (2006) Spontaneous neuronal activity
764 distinguishes human dorsal and ventral attention systems. Proceedings of the
765 National Academy of Sciences of the United States of America 103:10046-10051.
766 Fudge JL, Haber SN (2002) Defining the caudoventral striatum in primates: cytoarchitectural
767 and histochemical features. Journal of Neuroscience 22:10078-10082.
768 Fudge JL, Breitbart MA, McClain C (2004) Amygdaloid inputs define a caudal component of
769 the ventral striatum in primates. Journal of Comparative Neurology 476:330-347.
770 Fudge JL, deCampo DM, Becoats KT (2012) Revisiting the hippocampal-amygdala pathway
771 in primates: association with immature-appearing neurons. Neuroscience 212:104-
772 119.
773 Fudge JL, Breitbart MA, Danish M, Pannoni V (2005) Insular and gustatory inputs to the
774 caudal ventral striatum in primates. The Journal of comparative neurology 490:101-
775 118.
776 Fudge JL, Kunishio K, Walsh P, Richard C, Haber SN (2002) Amygdaloid projections to
777 ventromedial striatal subterritories in the primate. Neuroscience 110:257-275.
778 Geneser-Jensen FA, Blackstad TW (1971) Distribution of acetyl cholinesterase in the
779 hippocampal region of the guinea pig. Z Zellforsch 114:460-481.
780 Ghashghaei HT, Barbas H (2002) Pathways for emotion: interactions of prefrontal and
781 anterior temporal pathways in the amygdala of the rhesus monkey. Neuroscience
782 115:1261-1279.
783 Goldman-Rakic PS, Selemon LD (1986) Topography of corticostriatal projections in
784 nonhuman primates and implications for functional parcellation of the neostriatum.
785 In: Cerebral Cortex Vol. 5 (Jones EG, Peters A, eds), pp 447-466. New York: Plenum
786 Publishing Corporation.
787 Grabenhorst F, Baez-Mendoza R, Genest W, Deco G, Schultz W (2019) Primate Amygdala
788 Neurons Simulate Decision Processes of Social Partners. Cell 177:986-998 e915.
789 Gu Z, Gu L, Eils R, Schlesner M, Brors B (2014) circlize Implements and enhances circular
790 visualization in R. Bioinformatics 30:2811-2812.
791 Haber SN, Knutson B (2010) The reward circuit: linking primate anatomy and human
792 imaging. Neuropsychopharmacology : official publication of the American College of
793 Neuropsychopharmacology 35:4-26.
794 Haber SN, Fudge JL, McFarland N (2000) Striatonigrostriatal pathways in primates form an
795 ascending spiral from the shell to the dorsolateral striatum. Journal of Neuroscience
796 20(6):2369-2382.
797 Herzog AG, Van Hoesen GW (1976) Temporal neocortical afferent connections to the
798 amygdala in the rhesus monkey. Brain Res 115:57-69.
799 Hoffman RE, Fernandez T, Pittman B, Hampson M (2011) Elevated functional connectivity
800 along a corticostriatal loop and the mechanism of auditory/verbal hallucinations in
801 patients with schizophrenia. Biological psychiatry 69:407-414.
802 Jezzini A, Caruana F, Stoianov I, Gallese V, Rizzolatti G (2012) Functional organization of the
803 insula and inner perisylvian regions. Proceedings of the National Academy of Sciences
804 of the United States of America 109:10077-10082.

Karnath HO, Baier B (2010) Right insula for our sense of limb ownership and self-awareness of actions. Brain structure & function 214:411-417.
Klavir O, Genud-Gabai R, Paz R (2013) Functional connectivity between amygdala and cingulate cortex for adaptive aversive learning. Neuron 80:1290-1300.
Kordower JH, Piecinski P, Rakic P (1992) Neurogenesis of the amygdaloid nuclear complex in the rhesus monkey. Brain research Developmental brain research 68:9-15.
Likhtik E, Stujenske JM, Topiwala MA, Harris AZ, Gordon JA (2014) Prefrontal entrainment of amygdala activity signals safety in learned fear and innate anxiety. Nature neuroscience 17:106-113.
Meredith GE, Pattiselanno A, Groenewegen HJ, Haber SN (1993) Shell and core in the primate ventral striatum identified with antibodies against calbindin. Soc Neurosci Abst.
Mesulam M-M, Mufson EJ (1982) Insula of the Old World Monkey. I: Architectonics in the insulo-orbito-temporal component of the paralimbic brain. J Comp Neurol 212:1-22.
Mufson EJ, Mesulam MM, Pandya DN (1981) Insular interconnections with the amygdala in the rhesus monkey. Neuroscience 6:1231-1248.
Nieuwenhuys R, Voogd J, Huijzen CV (2007) Th Human Central Nervous System: A Synopsis and Atlas, 4 Edition: Springer.
Petrides M, Pandya DN (1999) Dorsolateral prefrontal cortex: comparative cytoarchitectonic analysis in the human and the macaque brain and corticocortical connection patterns. European Journal of Neuroscience 11:1011-1036.
Petrides M, Pandya DN (2002) Comparative cytoarchitectonic analysis of the human and the macaque ventrolateral prefrontal cortex and corticocortical connection patterns in the monkey. The European journal of neuroscience 16:291-310.
Popescu AT, Saghyan AA, Pare D (2007) NMDA-dependent facilitation of corticostriatal plasticity by the amygdala. Proceedings of the National Academy of Sciences of the United States of America 104:341-346.
Popescu AT, Popa D, Pare D (2009) Coherent gamma oscillations couple the amygdala and striatum during learning. Nature neuroscience.
Preuss TM, Goldman-Rakic PS (1991) Myelo-and cytoarchitecture of the granular frontal cortex and surrounding regions in the strepsirhine primate galago and the anthropoid primate macaca. J Comp Neurol 310:429-474.
Purves D, Lichtman JW (1980) Elimination of synapses in the developing nervous system. Science 210:153-157.
Ressler KJ (2020) Translating Across Circuits and Genetics Toward Progress in Fear- and Anxiety-Related Disorders. The American journal of psychiatry 177:214-222.
Robbins TW, Cador M, Taylor JR, Everitt BJ (1989) Limbic-striatal interactions in reward-related processes. Neuroscience & Biobehavioral Reviews 13:155-162.
Rose M (1928) Die inselrinde des menschen und der tiere. J Psychol Neurol 37:467-624.
Rosene DL, Roy NJ, Davis BJ (1986) A cryoprotection method that facilitates cutting frozen sections of whole monkey brains for histological and histochemical processing without freezing artifact. J Histochem Cytochem Vol. 34, No. 10:1301-1315.
Russchen FT, Bakst I, Amaral DG, Price JL (1985) The amygdalostriatal projections in the monkey. An anterograde tracing study. Brain Res 329:241-257.
Saez A, Rigotti M, Ostojic S, Fusi S, Salzman CD (2015) Abstract Context Representations in Primate Amygdala and Prefrontal Cortex. Neuron 87:869-881.

850 Saint-Cyr JA, Ungerleider LG, Desimone R (1990) Organization of visual cortical inputs to the
851 striatum and subsequent outputs to the pallido-nigral complex in the monkey. J Comp
852 Neurol 298:129-156.
853 Saunders RC, Rosene DL, Van Hoesen GW (1988) Comparison of the efferents of the
854 amygdala and the hippocampal formation in the rhesus monkey: II. Reciprocal and
855 non-reciprocal connections. J Comp Neurol 271:185-207.
856 Sengupta B, Faisal AA, Laughlin SB, Niven JE (2013) The effect of cell size and channel density
857 on neuronal information encoding and energy efficiency. J Cereb Blood Flow Metab
858 33:1465-1473.
859 Sherman SM, Guillery RW (1998) On the actions that one nerve cell can have on another:
860 Distinguishing "drivers" from "modulators". Proceedings of the National Academy of
861 Sciences of the United States of America 95:7121-7126.
862 Sliwa J, Freiwald WA (2017) A dedicated network for social interaction processing in the
863 primate brain. Science 356:745-749.
864 Stephan H, Frahm HD, Baron G (1987) Comparison of brain structure volumes in insectivora
865 and primates VII. Amygdaloid components. J Hirnforsch 5:571-584.
866 Van Hoesen GW, Yeterian EH, Lavizzo-Mourney R (1981) Widespread corticostriate
867 projections from temporal cortex of the rhesus monkey. J Comp Neurol 1981:205-
868 219.
869 Walker AE (1940) A cytoarchitectural study of the prefronal area of the macaque monkey. J
870 Comp Neurol 73:59-86.
871 Wilson FA, Scalaidhe SP, Goldman-Rakic PS (1993) Dissociation of object and spatial
872 processing domains in primate prefrontal cortex. Science 260:1955-1958.
873 Yeterian EH, Pandya DN (1995) Corticostriatal connections of extrastriate visual areas in
874 rhesus monkeys. Journal of Comparative Neurology 352:436-457.
875 Yeterian EH, Pandya DN (1998) Corticostriatal connections of the superior temporal region
876 in rhesus monkeys. Journal of Comparative Neurology 399:384-402.
877 Yeterian EH, Pandya DN, Tomaiuolo F, Petrides M (2012) The cortical connectivity of the
878 prefrontal cortex in the monkey brain. Cortex 48:58-81.
879

880 **Figure legends**

881 **Figure 1:** Study design**.** Cohort 1 animals (bi-directional tracer studies, purple) had a series of
882 injections placed in different subdivisions of the basal nucleus of the amygdala. Resulting retrogradely
883 labeled cells in the PFC and Insula were quantified; anterogradely labeled fibers in the striatum were
884 mapped to guide injections in Cohort 2. Cohort 2 animals (retrograde studies, orange) had a series
885 of injections placed in different regions of the striatum that were 'amygdala-recipient' (i.e. striatal
886 regions with labeled fibers in Cohort 1 animals). Retrogradely labeled cells in the amygdala, and the
887 PFC and Insula, were quantified.

888

889 **Figure 2:** Relative levels of cortical lamination in the PFC and Insula in the Macaque. ***A***. Ventral
890 view ***B***. Sagittal view from the midline ***C***. Lateral view, with lateral fissure 'opened' for ***C'.*** view of
891 insula. Image adapted from Carmichael & Price, 1994 and Saleem & Price, 2008. The key
892 illustrates the range of cortical differentiation; shades of blue indicate agranular cortex, shades of
893 green indicate dysgranular cortex, and shades of red indicate granular cortex. The darker the
894 shade within each granularity grouping indicates increased development of layer IV, layer II,
895 and/or layer V of cortex. Insets are from cresyl violet stained sections that give examples of
896 laminar regions in agranular, dysgranular and granular cortices. Bar = 500 um.
897 *Abbreviations: 6, area 6 (premotor/supplementary motor area); 8Ad, dorsal area 8A; 8Av,*
898 *ventral area 8A; 8B, area 8B; 9, area 9; 9m, medial area 9; 9/46d, dorsal area 9/46; 9/46v,*
899 *ventral area 9/46; 10m, medial area 10; 10o, orbital area 10; 11l, lateral area 11; 11m, medial*
900 *area 11; 12l, lateral area 12; 12m, medial area 12; 12o, orbital area 12; 12r, rostral area 12;*
901 *13a, area 13a; 13b, area 13b; 13l, lateral area 13; 13m, medial area 13; 14c, caudal area 14;*
902 *14r, rostral area 14; 24a, area 24a; 24b, area 24b; 24c, area 24c; 25c, caudal area 25; 25r,*
903 *rostral area 25; 32c, caudal area 32; 32r, rostral area 32, 45, area 45; 46, area 46; 9/46d,*
904 *dorsal area 9/46; area 9/46v, ventral area 9/46; cc, corpus callosum; G, gustatory cortex; Iai,*
905 *intermediate agranular insula area; Ial, lateral agranular insula area; Iam, medial agranular*
906 *insula area; Iapl, posterolateral agranular insula area; Iapm, posteromedial agranular insula*
907 *area; Id, dysgranular insula; Ig, granular insula; ob, olfactory bulb; oc, optic chiasm; PrCO,*
908 *precentral opercular area.*
909

910 **Table 1:** Laminar characteristics of the PFC and insula subdivisions, and 3- and 9-group
911 granularity assignments. Each column indicates the main granularity grouping of every
912 Brodmann's area examined (i.e. the relative thickness of layer IV of cortex). The darker the

913 shade within each sub-section within each column (i.e. 'Agranular 1' vs. 'Agranular 2') represents
914 the increasing degree of layer V sublamination and/or layer IV development within each
915 granularity assignment.
916
917 **Figure 3:** Schematic of injection site locations in basal nucleus. ***A***. Injection site locations (gray)
918 in rostro-central Bmc, Bi, and Bpc. ***B***. Injection site locations (gray) in caudal Bpc. ***C***. Dark-field
919 photomicrograph of injection site location for J16LY, indicated with a white arrow. ***D***. Adjacent
920 AChE-stained section matched to ***C.*** to localize injection to basal nucleus subdivision (Bmc). ***E***.
921 Dark-field photomicrograph of the injection site location for J47FS, indicated with a white arrow.
922 ***F***. Adjacent AChE-stained section matched to ***E.*** to localize injection site within basal nucleus
923 subdivision (Bi). ***G.*** Dark-field photomicrograph of the injection site location for J15FS, indicated
924 with a white arrow. ***H.*** Adjacent AChE-stained section matched to ***H.*** to localize injection site
925 within basal nucleus subdivision (Bpc). Photos taken at 2x magnification. Scale bars = 500 μm.
926 *Abbreviations: AB, accessory basal nucleus; Bi, intermediate basal nucleus; Bmc, magnocellular*
927 *basal nucleus; Bpc, parvicellular basal nucleus; L, lateral nucleus; P, putamen; V, ventricle.*
928
929 **Figure 4:** Cortico-amygdala path. ***A.*** Representative charts showing the pattern of retrogradely
930 labeled cells in the PFC and insula resulting from 6 non-overlapping injection sites along the
931 dorsal-ventral extent of the basal nucleus. ***a'.*** The photomicrograph inset shows an example of
932 densely concentrated retrogradely labeled cells in the Ial of J15FS. Scale bar = 100 μm ***B.***
933 Chord diagram showing quantitative analysis of all retrogradely labeled cells (1:24 sections)
934 through PFC and insula, classified by laminar differentiation. The top axis of this diagram shows
935 the total number of labeled cells in agranular (blue), dysgranular (green), and granular (red)
936 cortical areas across all cases examined. The bottom axis shows the number of labeled cells in
937 agranular, dysgranular, and granular cortices resulting from each basal nucleus injection site.

938 Injection sites are arranged counter-clockwise from the most caudal-ventral (left) to most rostral-
939 dorsal injection site location (right). 1 tick mark= 180 cells.
940 *Abbreviations: AC, anterior commissure; C, caudate; cc, corpus callosum; IC, internal capsule;*
941 *oc, optic chiasm; NA, nucleus accumbens; P, putamen, V, ventricle. For cortical abbreviations,*
942 *see "Abbreviations" in Figure 2 legend.*
943
944 **Extended Figure 4-1:** Cortico-amygdala chord diagram showing additional quantitative analysis
945 of retrograde labeling using 9-group granularity analysis. The top axis shows the total number of
946 labeled cells in agranular (3 shades of blue), dysgranular (3 shades of green), and granular (3
947 shades of red) cortical areas across all cases examined. The darker the shade within each
948 granularity grouping indicates increased development of layer IV, layer II, and/or layer V of
949 cortex. The bottom axis of this diagram shows the number of labeled cells from each granularity
950 subgroup that results from each basal nucleus injection site. The bottom axis is organized
951 counter-clockwise by most caudal-ventral (left) to most rostral-dorsal (right) injection site
952 location. Each tic mark for both the top and bottom axes represents 180 cells.
953
954 **Figure 5:** Representative charts showing distribution of anterogradely labeled fibers resulting
955 from the same 6 non-overlapping injection sites shown in Fig. 4, along the dorsal-ventral extent
956 of the basal nucleus. Injection sites arranged from caudo-medial (Bpc) to rostro-dorsal (Bmc)
957 across the top. Striatal section are organized from rostral to caudal levels under each injection
958 site. Photomicrograph inset shows high density patch of labeled fibers in the caudal ventral
959 putamen (darkfield). Bar = 500 μm.
960 *Abbreviations: AC, anterior commissure; C, caudate; C(g), genu of the caudate nucleus; C(t),*
961 *tail of the caudate nucleus; GP, globus pallidus; GPe; external globus pallidus; GPi, internal*
962 *globus pallidus; IC, internal capsule; lAstr, lateral amygdalostriatal area; LGN, lateral geniculate*

963 *nucleus; lIPAC, lateral interstitial nucleus of the posterior limb of the anterior commissure; mAstr,*
964 *medial amygdalostriatal area; mIPAC, medial interstitial nucleus of the posterior limb of the*
965 *anterior commissure; OT, optic tract; P, putamen; V, ventricle.*
966
967 **Figure 6:** Striatal Injection sites in Cohort 2. ***A. - D.*** Schematics of retrograde injection site
968 locations from the rostral (A) to progressively caudal regions (B-D). Medium gray sites (solid
969 lines) depict injections with significant labeled cells in amygdala, included for analysis; light gray
970 sites (dotted lines) resulted in few labeled cells in the amygdala. ***E-F.*** Brightfield
971 photomicrographs in the classic ventral striatum. ***E***. Injection site location in dorsomedial shell,
972 with adjacent CaBP-stained section (***E'.***) showing injection alignment in CaBP-negative shell**.** ***F.***
973 Injection site in the rostral 'core', with adjacent CaBP-stained section (**F'**.) showing shell/core
974 boundary. ***G-J****.* Caudal 'limbic' striatum injection sites. ***G.*** caudoventral putamen at the level of
975 the anterior commissure, ***H.*** caudoventral putamen posterior to the anterior commissure. ***I.***
976 ventral body of caudate nucleus **.** ***J.*** Injection site location in caudomedial putamen at the level
977 of the hippocampus. Scale bars = 1mm.
978 *Abbreviations: AC, anterior commissure; C, caudate; Co, ventral striatum core; GPe; external*
979 *globus pallidus; GPi, internal globus pallidus; IC, internal capsule; P, putamen; Sh, ventral*
980 *striatum shell.*
981
982 **Figure 7:** Amygdalo-striatal path. ***A.*** Charts of retrogradely labeled cells through the
983 rostrocaudal basal nucleus following injections in Cohort 2. Injection sites arranged from rostral
984 (top) to caudal (bottom). All 6 cases resulted in many retrogradely labeled cells in the basal
985 nucleus. Cell labeling in other nuclei (shaded in gray) is not shown for clarity. ***B.*** Chord diagram
986 showing numbers of labeled cells in the Bpc, Bi, and Bpc by injection site placement. The top
987 axis of this diagram shows the total number of labeled cells in Bpc (cyan), Bi (fuchsia), and Bmc
988 (purple) across all cases examined. The bottom axis shows the number of labeled cells in each

989 basal nucleus subdivision resulting from each striatal injection site, and is arranged counter-
990 clockwise from the most rostral (left) to most caudal (right) injection site location. Each tick mark
991 for both the top and bottom axes = 60 cells.
992
993 **Figure 8:** Cortico-'limbic' striatal path. ***A.*** Representative charts depicting retrogradely labeled
994 cells in the PFC and insula after injections in various striatal regions along the rostral-caudal
995 extent of the 'limbic' striatum. Cases J24WGA and J13WGA had injections in shell and core of
996 the 'classic' ventral striatum, respectively. Injection sites in J8WGA, J12WGA, J41WGA, and
997 J11WGA were placed in different parts of the 'extended' ventral striatum. ***B.*** Chord diagram
998 showing the number of retrogradely labeled cells in agranular (blue), dysgranular (green), and
999 granular (red) cortical areas across all cases examined (top axis). The bottom axis shows the
1000 number of labeled cells found in agranular, dysgranular, and granular cortices after each striatal
1001 injection site. The bottom axis is arranged counter-clockwise from the most rostral (left) to the
1002 most caudal (right) injection site location. Each tick mark represents 400 cells.
1003
1004 **Figure 8-1** : Cortico-striatal chord diagram showing additional quantitative analysis of retrograde
1005 labeling using 9-group granularity analysis. The top axis of this diagram follows the same color
1006 schema as described in **Figure 4-1.** The bottom axis of this diagram shows the number of
1007 labeled cells from each granularity subgrouping that results from each striatal injection site. The
1008 bottom axis is organized counter-clockwise by most rostral (left) to most caudal (right) injection
1009 site location. Each tic mark for both the top and bottom axes represents 400 cells.
1010
1011 **Figure 9:** Indirect and direct pathway analysis**.** ***A.*** Composite diverging bar plots of each striatal
1012 injection showing the proportion of labeled cells in agranular (blue), dysgranular (green) and
1013 granular (red) cortices after calculating indirect pathway and direct pathway labeled cells. The

1014 proportion of labeled cells associated with amygdala inputs to all striatal sites ('indirect' path) is
1015 relatively consistent with a large percentage of cells categorized as agranular, and consistently
1016 small percentages of labeled cells categorized as dysgranular and granular, respectively. In
1017 contrast, the 'direct' cortico-'limbic' striatal path shows more variation with rostral ventral striatal
1018 sites having the greatest proportion of labeled cells in agranular cortices, and relatively small
1019 contributions from the dysgranular and granular cortices. This balance shifts at progressively
1020 caudal ventral levels, with reductions in labeled cells in agranular cortices, and incrementally
1021 more labeled cells in dysgranular cortices > granular cortices. ***B.*** Individual cases plotted for
1022 each path.
1023
1024 **Figure 10:** Brodmann's classification. ***A.*** Additional quantitative analysis of retrograde cortico-
1025 amygdala cell labeling using Brodmann's classification. The top axis of this diagram shows the
1026 total number of labeled cells in Brodmann's areas examined. Blue indicates this Brodmann's
1027 area is exclusively agranular cortex, blue-green indicates this Brodmann's area contains a mix
1028 of agranular and dysgranular cortex, green indicates this Brodmann's area is exclusively
1029 dysgranular cortex, orange indicates this Brodmann's area contains a mix of dysgranular and
1030 granular cortex, and red indicates this Brodmann's area is exclusively granular cortex. The
1031 bottom axis of this diagram shows the number of labeled cells from each Brodmann's area that
1032 results from each basal nucleus injection site. The bottom axis is organized counter-clockwise
1033 by most caudal-ventral (left) to most rostral-dorsal injection (right) injection site location. Each tic
1034 mark for both the top and bottom axes represents 180 cells. ***B.*** Additional quantitative analysis
1035 of retrograde cortico-striatal cell labeling using Brodmann's classification, indicated on the top
1036 axis. The same color schema describe in ***A.*** applies here. The bottom axis of this diagram shows
1037 the number of labeled cells from each granularity subgrouping that results from each striatal
1038 injection site. The bottom axis is organized counter-clockwise by most rostral (left) to most caudal
1039 (right) injection site location. Each tic mark for both the top and bottom axes represents 400

1040 cells.

1041

1042 **Figure 11:** Overview of 'cortical logic' in the 'indirect' pathway (PFC/Insula → amygdala
1043 connectivity, left + amygdala → 'limbic' striatum connectivity , bottom) and the 'direct' pathway
1044 (PFC/Insula → 'limbic' striatum connectivity, right).

1045 ***Supplemental Methods***

1046 ***Brodmann's areas (Fig. 2)***

1047 *Ventromedial Prefrontal cortex (vmPFC) and dmPFC.* The medial prefrontal cortex
1048 (mPFC) is comprised of the medial frontopolar cortices, the cortex of the superior frontal
1049 gyrus, anterior cingulate, and the gyrus rectus, which gradually transition from granular
1050 cortex in the frontal poles to agranular cortex in the ventral anterior cingulate. Behind the
1051 frontopolar mPFC (granular area 10m), the dmPFC contains medial aspects of
1052 dysgranular areas 9 and 8B, which continue onto the lateral convexity (Figs. 2A & 2B)
1053 (Walker, 1940; Preuss and Goldman-Rakic, 1991; Petrides and Pandya, 1999). These
1054 regions are dorsal to the anterior cingulate cortex. The cingulate cortex, which includes
1055 areas 24a-c, 32, and 25, are all agranular. Out of these areas, ventral area 25 is the least
1056 differentiated (Carmichael and Price, 1994; Nieuwenhuys et al., 2007). Areas 32 and 24
1057 are relatively more differentiated rostrally and dorsally, respectively. Similarly, area 14
1058 granularity changes through its rostral-caudal extent. Area 14r is dysgranular cortex,
1059 while areas 14c is agranular cortex (Carmichael and Price, 1994).

1060 *OFC.* The OFC houses one agranular subdivision (area 13a), but is largely composed
1061 of dysgranular and granular subdivisions (Fig. 2C). The most rostral extent of OFC is

1062 composed of dysgranular area 12r and granular areas 10o (frontal pole), 11m, and 11l.
1063 Posterior to these regions are granular area 12m and dysgranular areas 13b, 13m, and
1064 13l. The most posterior reaches of the OFC, which form a continuum with the insula, are
1065 dysgranular area 12o and agranular area 13a.
1066
1067 *vlPFC and dlPFC.* The vlPFC is composed of areas 45 and 12l (Walker, 1940; Preuss
1068 and Goldman-Rakic, 1991; Carmichael and Price, 1994; Petrides and Pandya, 2002)
1069 (Figs. 2A and 2C). Both areas 45 and 12l are granular, but area 45 is more differentiated
1070 than area 12l. The dlPFC is composed of areas 8B, 8Ad, 8Av, 9, 9/46d, 9/46v, and 46
1071 (Figs. 2A and 2B), and is contiguous with the underlying vlPFC (Fig. 2B). It is considered
1072 isocortex, but it also contains a gradient of differentiation. Area 8B is mostly contained in
1073 the dlPFC, but also descends into the medial wall (Fig. 2A). Area 8B and area 9 have a
1074 poorly distinguished layer IV, and are the only dysgranular areas within the
1075 overwhelmingly granular dlPFC (Preuss and Goldman-Rakic, 1991; Petrides and
1076 Pandya, 1999); The other regions of the dlPFC (areas 46, 9/46, and 8A) are granular
1077 cortex. Area 46 is found in the rostral-most extent of the sulcus principalis. Area 9/46 is
1078 more caudal than area 46, and is divided into a dorsal (9/46d) and a ventral (9/46v)
1079 component based on its relative position along the sulcus principalis. Areas 8Ad and 8Av
1080 are generally more caudal (and lateral) than areas 46, 9/46d, & 9/46v, have a broad and
1081 densely packed layer IV, and are the most highly differentiated PFC regions.
1082
1083 *Insula.* The anterior insula forms a continuum with the OFC, and resides on the caudal
1084 orbital surface (Rose, 1928; Carmichael and Price, 1994; Nieuwenhuys et al., 2007) (also

1085 known as ‘proisocortex’ in other studies (Barbas and Pandya, 1989)). Here, the agranular
1086 insula is composed of several subdivisions, with the most undifferentiated being the
1087 posteromedial insula (Iapm) and anterior medial insula (Iam), with slightly more
1088 differentiated agranular regions (the intermediate insula (Iai), lateral insula (Ial), and
1089 posterolateral agranular insula (Iapl)) found most laterally (Carmichael and Price, 1994)
1090 (Figs. 2C & 2D). Progressing into the bank of the Sylvian fissure, the ventral insula is
1091 agranular, with progressively more differentiated insula found dorsally (Fig. 2D).

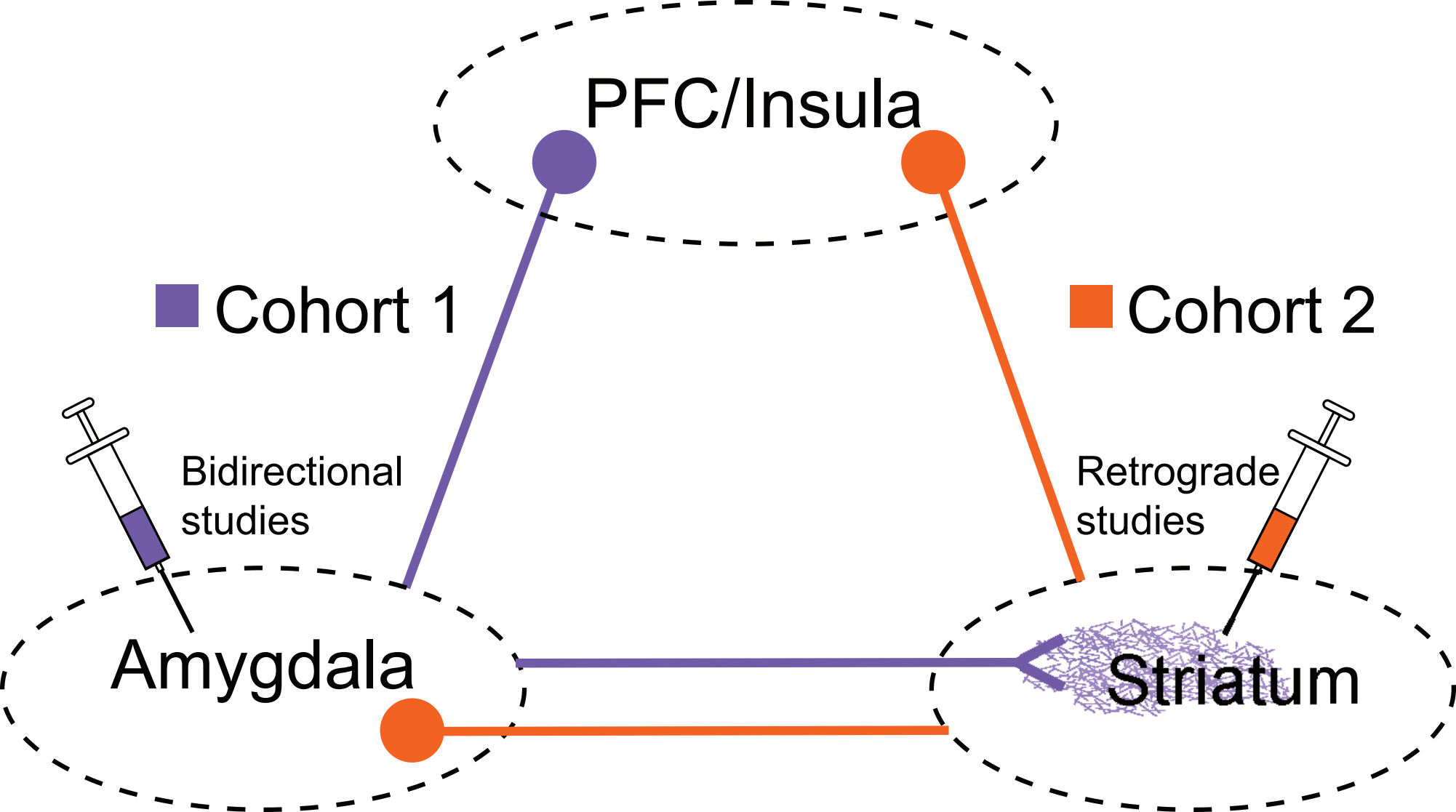
PFC/Insula
Cohort 1
Cohort 2
Bidirectional studies
Retrograde studies
Amygdala
Striatum

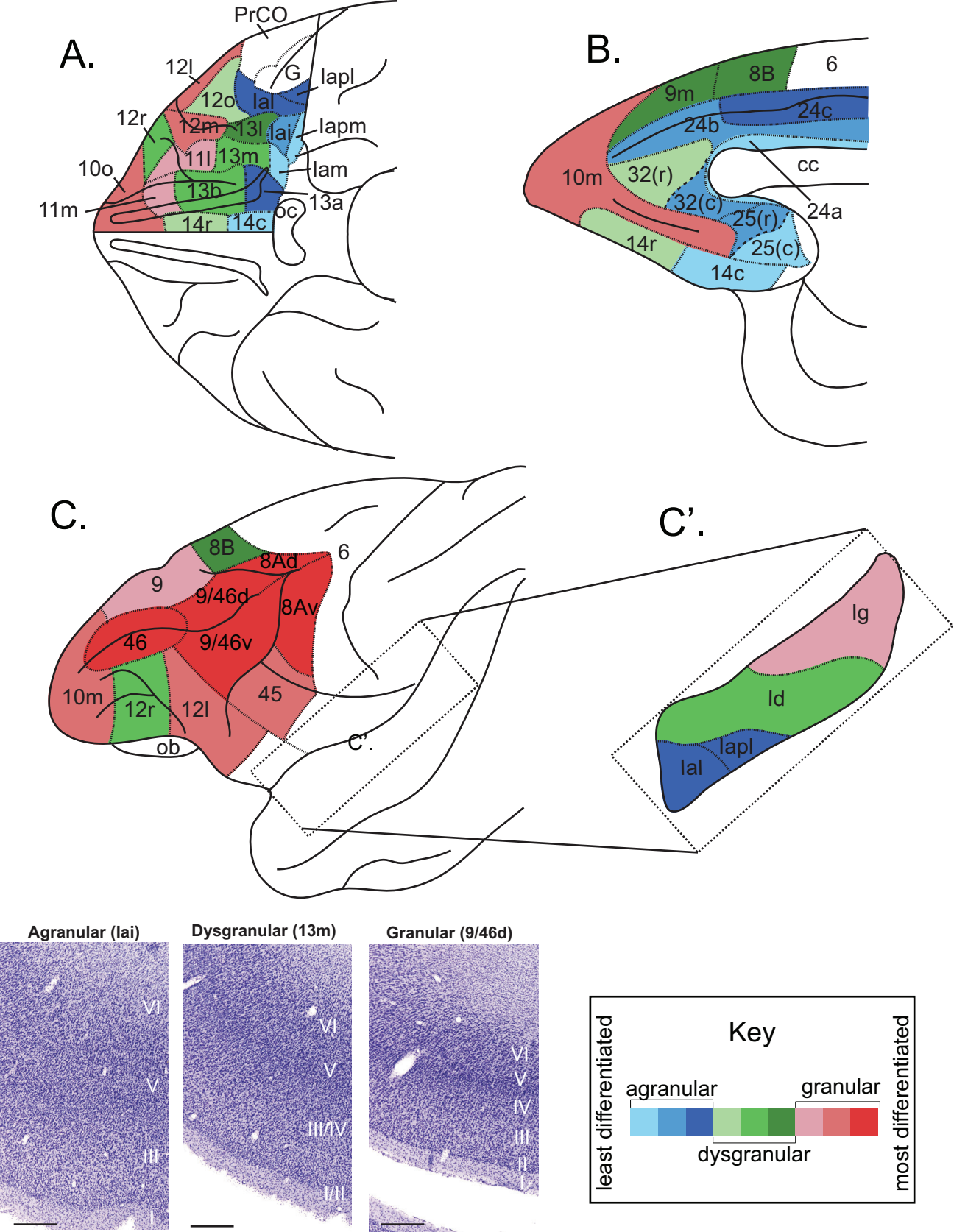
A.
PrCO
12l
G
lapl
12o
lal
12r
12m
13l
lai
lapm
11l
13m
10o
lam
13b
11m
13a
14r
14c
oc
B.
6
8B
9m
24c
24b
cc
10m
32(r)
32(c)
24a
25(r)
14r
25(c)
14c
C.
8B
8Ad
6
9
9/46d
8Av
46
9/46v
10m
12r
12l
45
ob
C'.
C'.
Ig
Id
lapl
lal
Agranular (lai)
Dysgranular (13m)
Granular (9/46d)
VI
V
III
I
VI
V
III/IV
I/II
VI
V
IV
III
II
I
Key
least differentiated
most differentiated
agranular
granular
dysgranular

Table 1: Rationale for 3- and 9-group granularity assignments

Agranular	
Granularity Grouping	Reason for granularity grouping
Agranular 1	
Iam	No layer IV, and no layer V sublamination. (Carmichael & Price, 1994)
Iapm	No layer IV, and no layer V sublamination. (Carmichael & Price, 1994)
25c	No layer IV, less developed compared to 32c, 32r, and 25r. (Carmichael & Price, 1994)
24a	Has only 4 cortical layers and rudimentary lamination. (Carmichael & Price, 1994)
14c	Has only 4 cortical layers. (Carmichael & Price, 1994)
Agranular 2	
32c	No layer IV; Caudal 32 resembles 25r; has horizontal striations of pyramidal cells in layer V. (Carmichael & Price, 1994)
25r	No layer IV; caudal 32 resembles 25r. (Carmichael & Price, 1994)
24b	No layer IV; has more prominent vertical striations in layer V compared to 24c. (Carmichael & Price, 1994)
Iai	No layer IV; has partially sublaminated layer V; superficial layer V has row of large pyramidal cells. (Carmichael & Price, 1994)
Agranular 3	
Ial	No layer IV; layer V is sublaminated. (Carmichael & Price, 1994)
Iapl	No layer IV; layer V is sublaminated. (Carmichael & Price, 1994)
13a	No layer IV; layer V is sublaminated. (Carmichael & Price, 1994)
24c	No layer IV; Has pyramidal cell aggregates in layer V. (Carmichael & Price, 1994)

Dysgranular	
Granularity Grouping	Reason for granularity grouping
Dysgranular 1	
32r	Is more developed than 32c and 25r and is slightly dysgranular (Carmichael & Price, 1994). No layer V sublamination.
12o	Very weakly staining layer IV, no layer V sublamination. (Carmichael & Price, 1994)
14r	Has distinct small cells in layer II, no horizontal or vertical striations in layer V. (Carmichael & Price, 1994)
Dysgranular 2	
13b	Has horizontal and vertical striations in layer V. (Carmichael & Price, 1994)
12r	Has vertical striations in layer V, but it is not sublaminated. (Carmichael & Price, 1994)
13m	Has a sparse granular layer. Has no/less distinct sublamination of layer V (and layer III). (Carmichael & Price, 1994)
Id	Has thin layer IV with clusters of granular cells interrupted by pyramidal cells. No layer II. Almost identical in appearance to dysgranular component of caudal OFC. (Mesulam & Mufson, 1982)
Dysgranular 3	
13l	Has poorly developed layer IV and has clearly sublaminated layer V. (Carmichael & Price, 1994)
8B	Layer II is well defined; Layer IV is poorly developed and layer V blends with layer VI, but layer V is sublaminated (it has a few darkly stained cells in layer Va). (Petrides & Pandya, 1999)
9m	Has a more narrow and cell sparse layer IV than 9. (Petrides & Pandya, 1999)

Granular	
Granularity Grouping	Reason for granularity grouping
Granular 1	
9	Has a narrow layer IV. Layer Va has deeply pigmented cells and layer Vb blends with layer VI. (Petrides & Pandya, 1999)
Ig	Layer II has moderately advanced granularity, and layer IV has prominent granularity. Layer V and VI are not fully differentiated from each other; (Layer III is bilaminate).(Mesulam & Mufson, 1982)
11m	Granular with bilaminate layer V. Layer V is thinner and more trilaminate than in 13m. Outer and inner sublaminae are broken into aggregates of neurons. (Carmichael & Price, 1994)
11l	Granular with bilaminate layer V containing aggregates of pyramidal cells. Layer V is thinner and more trilaminate than in 13m. Does not have outer and inner sublaminae broken up into neuron aggregates. (Carmichael & Price, 1994)
Granular 2	
10o	Is more granular than 11m and 11l, but layer IV not as clear. Layer V is thinner than in 11m or 11l; contains vertical and horizontal striations in layer V, and layer V is thinner than 11l and 11m. (Carmichael & Price, 1994)
10m	Has completely developed II and IV; has horizontal and vertical striations in layer V. Layer IV is more granular than 11m and 11l but not well demarcated, thin layer V with radial striations. (Carmichael & Price, 1994)
12m	Has completely developed II and IV; has clearly sublaminated layer V. Is more granular than 12r, 13l, and 12o. (Carmichael & Price, 1994)
12l	Has completely developed layers II and IV; has prominent/sharp sublamination of layer V. (Carmichael & Price, 1994)
45	Well developed layer IV with medium sized layer V (also has distinct and uniquely thick layer III). (Petrides & Pandya, 2001)
Granular 3	
8Av	Layer IV is broad and densely packed with small neurons (Layer II is also developed and densely packed). Layer V is less dense, but is bilaminate. Resembles 8Ad, but layer IV is broader, and layer III pyramidal neurons are more densely packed. (Petrides & Pandya, 1999)
8Ad	Layer IV is broad and densely packed with small neurons (Layer II is also developed and densely packed). Layer V is less dense, but is bilaminate. Resembles 8Av, but layer IV is less broad, and layer III pyramidal neurons are less densely packed. (Petrides & Pandya, 1999)
46	Layer IV is well developed; layer V is sublaminated (layer Va has small number of deeply stained cells and layer Vb blends with layer VI). (Petrides & Pandya, 1999)
9/46d	Similar features as 46, but layer III has large and darkly stained pyramidal neurons; Located dorsally. (Petrides & Pandya, 1999)
9/46v	Similar features as 46, but layer III has large and darkly stained pyramidal neurons; Located ventrally. (Petrides & Pandya, 1999)

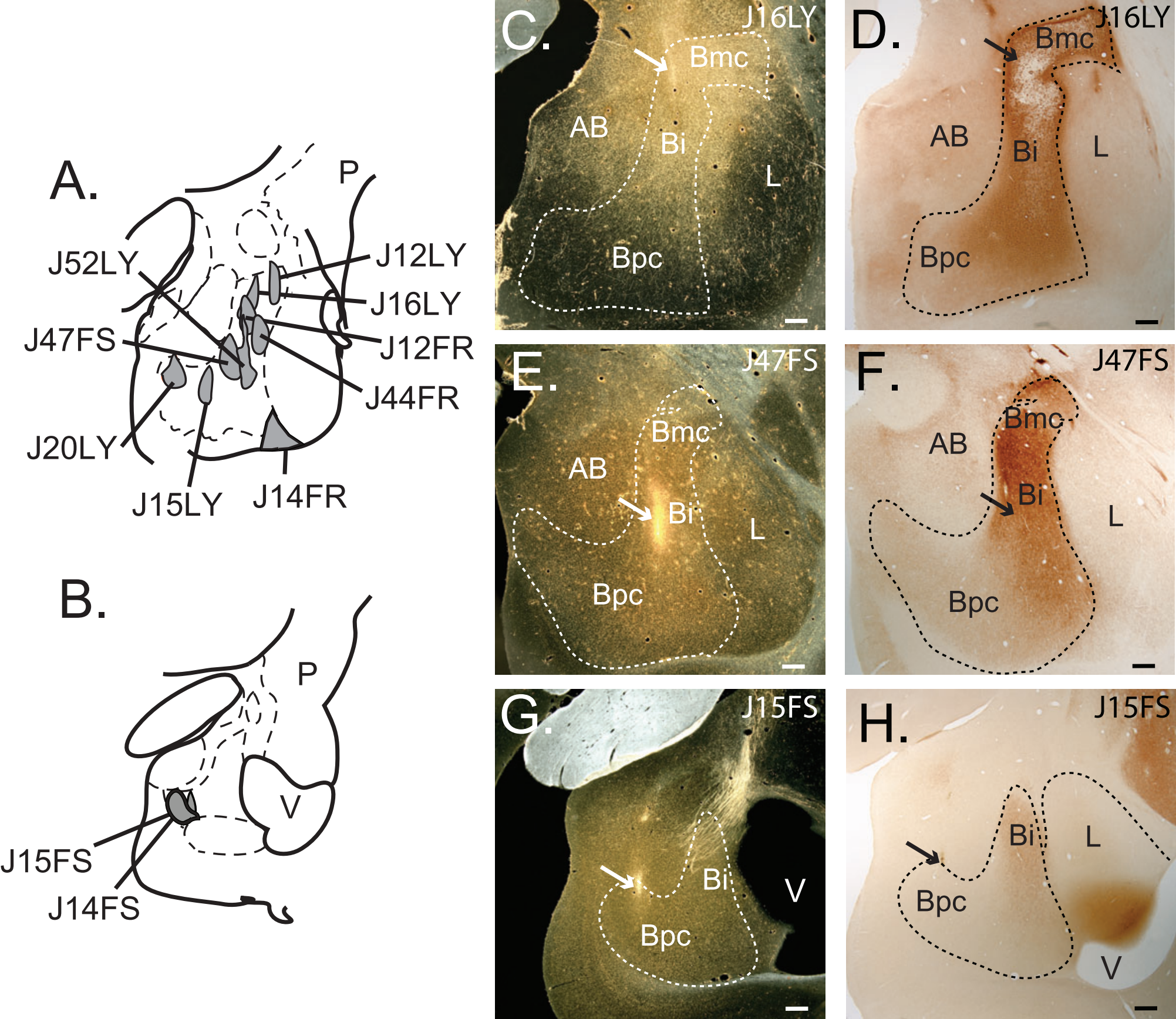
A.
P
J52LY
J12LY
J16LY
J47FS
J12FR
J44FR
J20LY
J15LY
J14FR
B.
P
V
J15FS
J14FS
C.
J16LY
Bmc
AB
Bi
L
Bpc
D.
J16LY
Bmc
AB
Bi
L
Bpc
E.
J47FS
Bmc
AB
Bi
L
Bpc
F.
J47FS
Bmc
AB
Bi
L
Bpc
G.
J15FS
Bi
V
Bpc
H.
J15FS
Bi
L
Bpc
V

A.

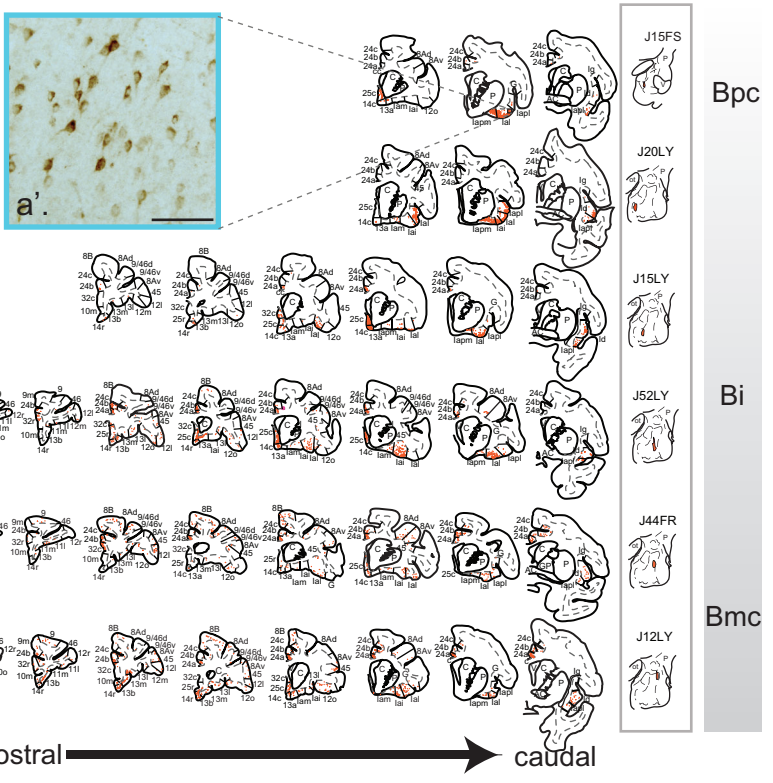
a'.
J15FS
J20LY
J15LY
J52LY
J44FR
J12LY
Bpc
Bi
Bmc
rostral
caudal

B.

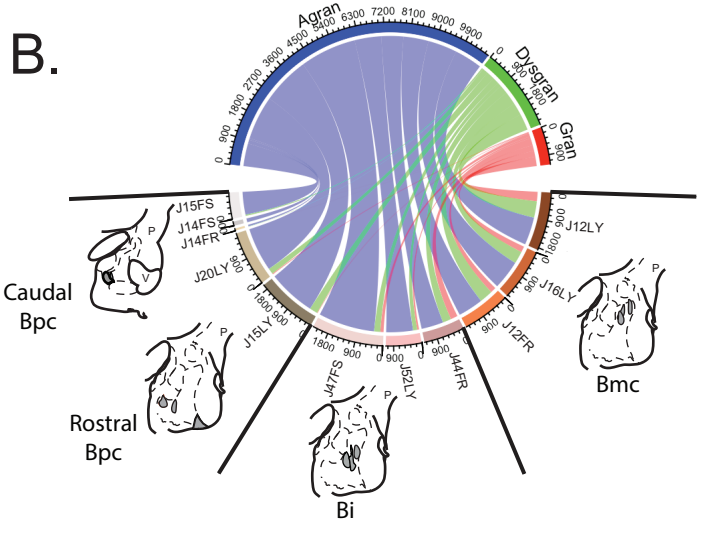
Agran
Dysgran
Gran
J15FS
J14FS
J14FR
J20LY
J15LY
J47FS
J52LY
J44FR
J12FR
J16LY
J12LY
Caudal Bpc
Rostral Bpc
Bi
Bmc

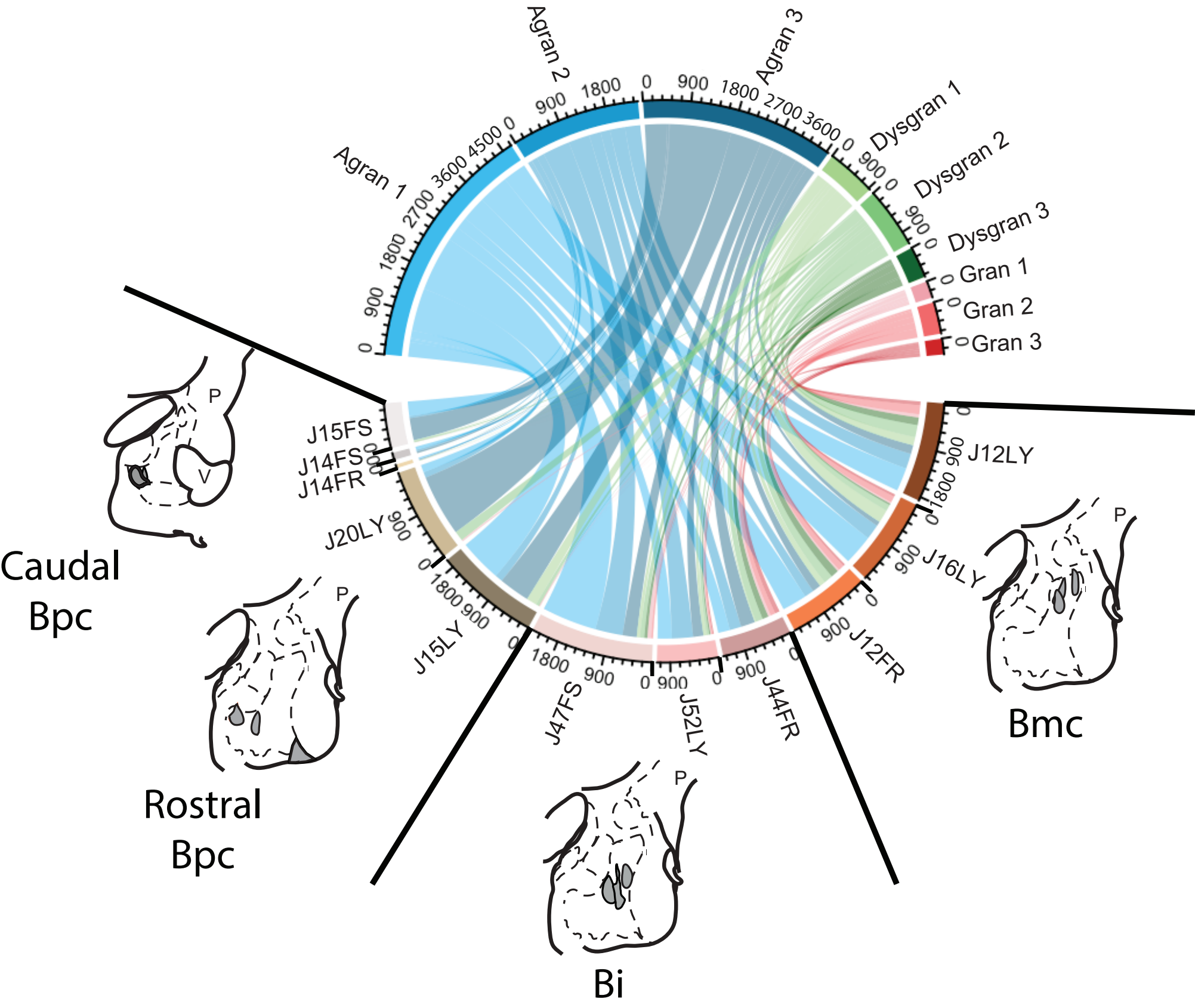
Agran 1
Agran 2
Agran 3
Dysgran 1
Dysgran 2
Dysgran 3
Gran 1
Gran 2
Gran 3
J15FS
J14FS
J14FR
J20LY
J15LY
J47FS
J52LY
J44FR
J12FR
J16LY
J12LY
Caudal Bpc
Rostral Bpc
Bi
Bmc
P
V

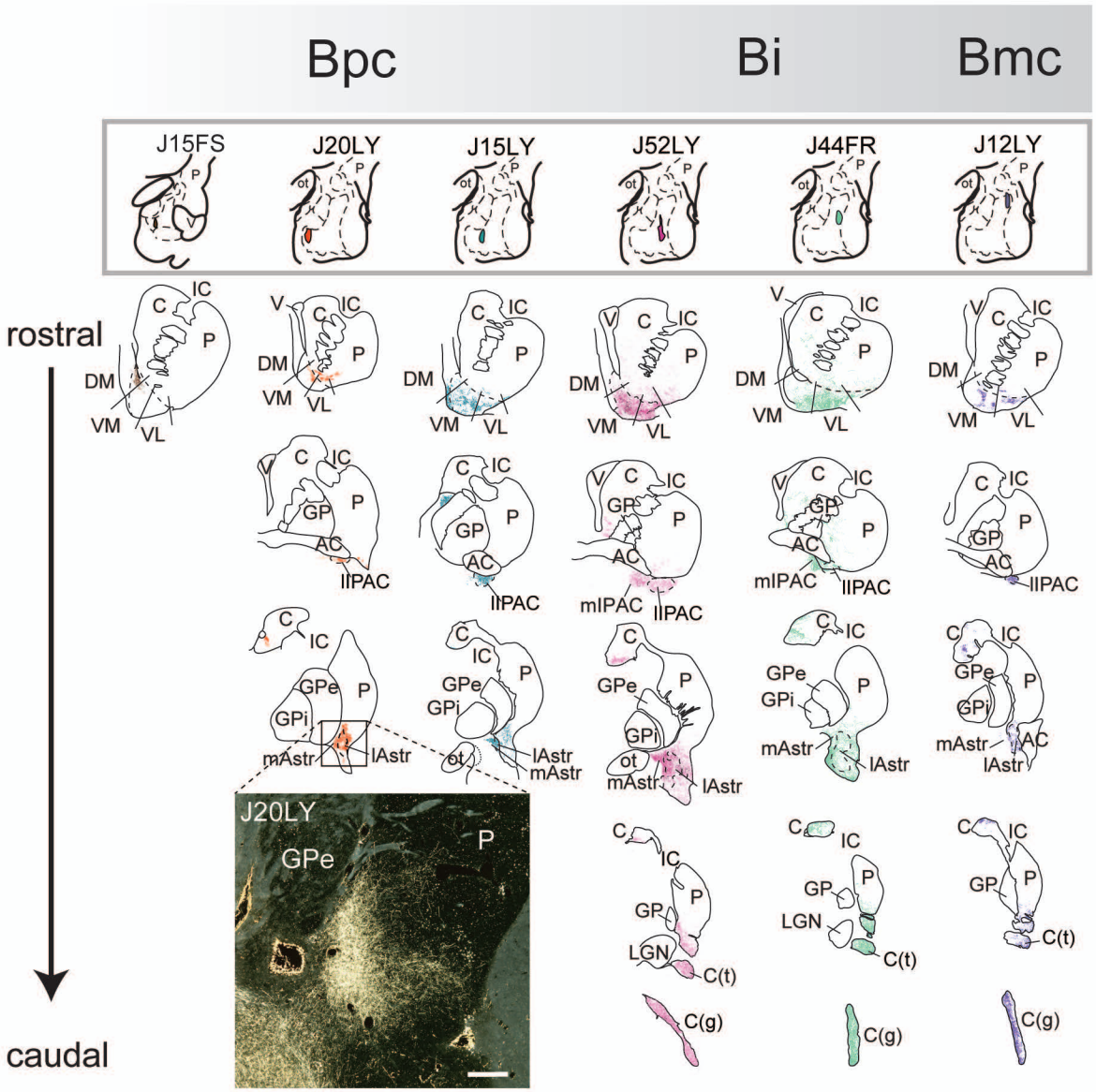
Bpc
Bi
Bmc
J15FS
J20LY
J15LY
J52LY
J44FR
J12LY
rostral
caudal
IC
C
P
V
DM
VM
VL
GP
AC
lIPAC
mIPAC
GPe
GPi
mAstr
lAstr
ot
LGN
C(t)
C(g)
J20LY
GPe
P

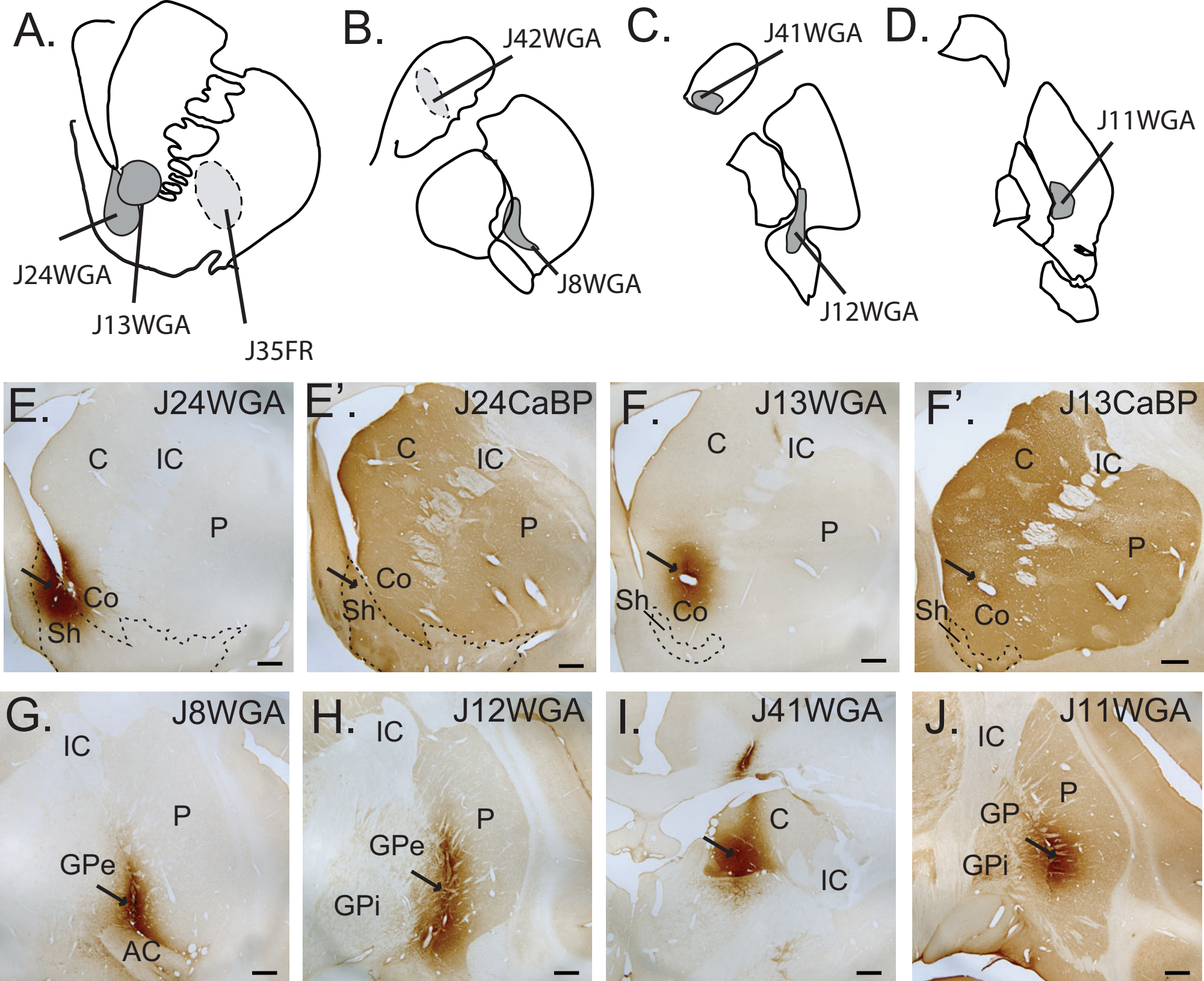
A.
J24WGA
J13WGA
J35FR
B.
J42WGA
J8WGA
C.
J41WGA
J12WGA
D.
J11WGA
E.
J24WGA
C
IC
P
Co
Sh
E'.
J24CaBP
C
IC
P
Co
Sh
F.
J13WGA
C
IC
P
Sh
Co
F'.
J13CaBP
C
IC
P
Sh
Co
G.
J8WGA
IC
P
GPe
AC
H.
J12WGA
IC
P
GPe
GPi
I.
J41WGA
C
IC
J.
J11WGA
IC
P
GP
GPi

A.

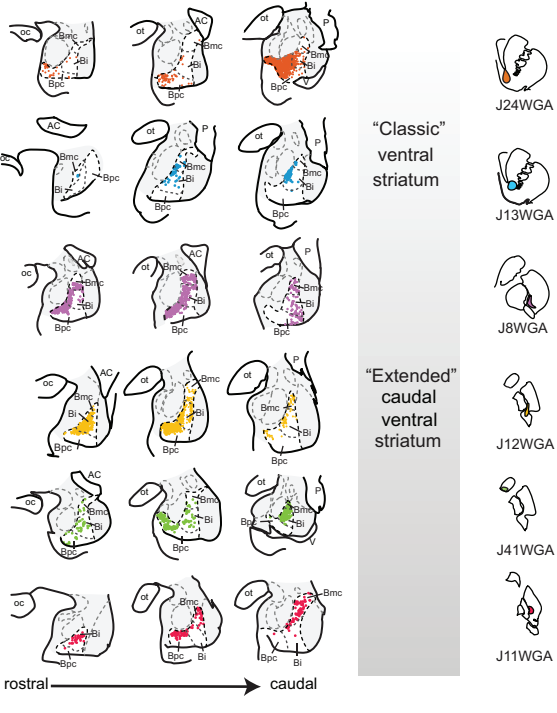
"Classic" ventral striatum
"Extended" caudal ventral striatum
J24WGA
J13WGA
J8WGA
J12WGA
J41WGA
J11WGA
rostral
caudal

B.

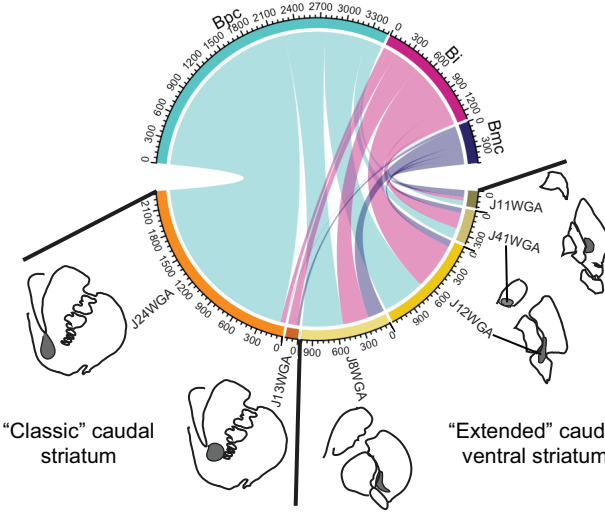
Bpc
Bi
Bmc
J11WGA
J41WGA
J12WGA
J8WGA
J13WGA
J24WGA
"Classic" caudal striatum
"Extended" caudal ventral striatum

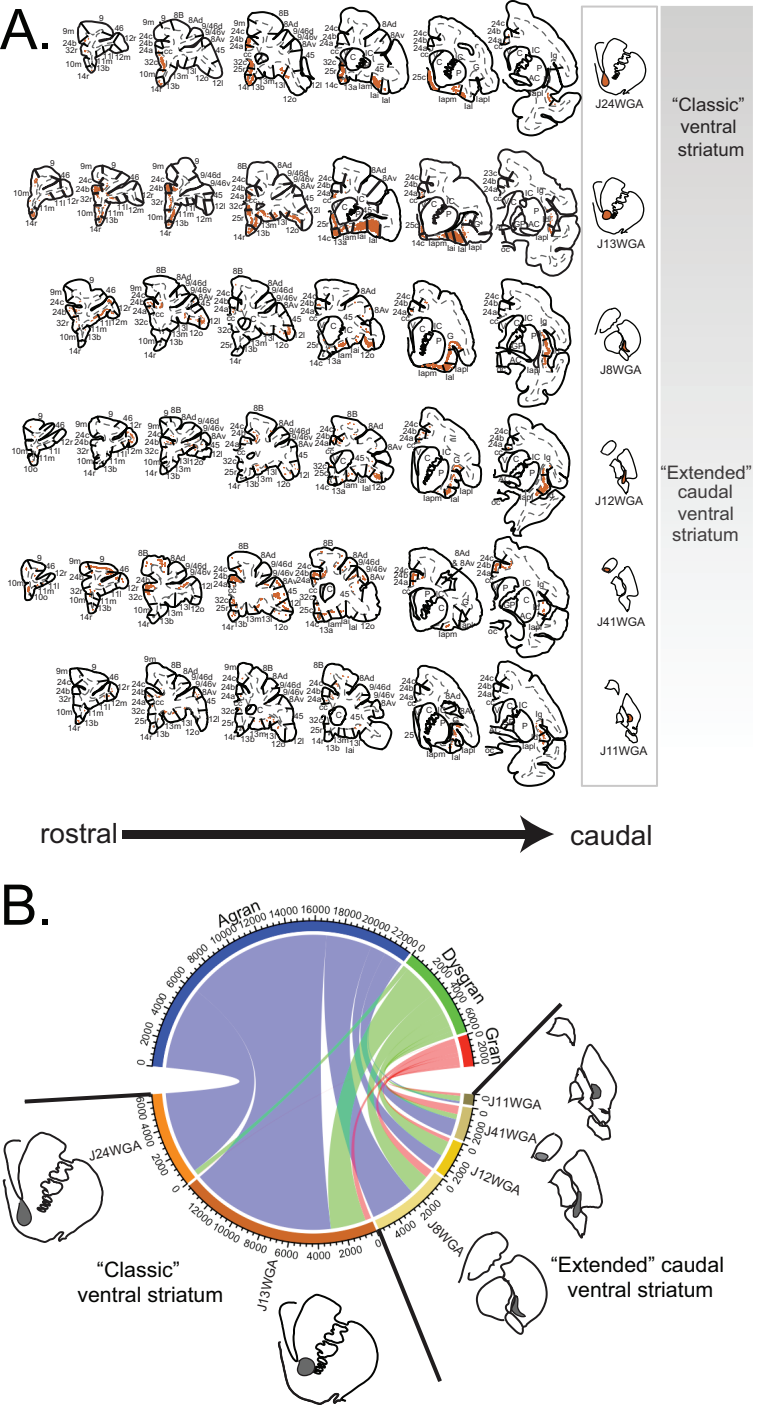
A.
J24WGA
J13WGA
J8WGA
J12WGA
J41WGA
J11WGA
"Classic" ventral striatum
"Extended" caudal ventral striatum
rostral
caudal
B.
Agran
Dysgran
Gran
J11WGA
J41WGA
J12WGA
J8WGA
J13WGA
J24WGA
"Classic" ventral striatum
"Extended" caudal ventral striatum

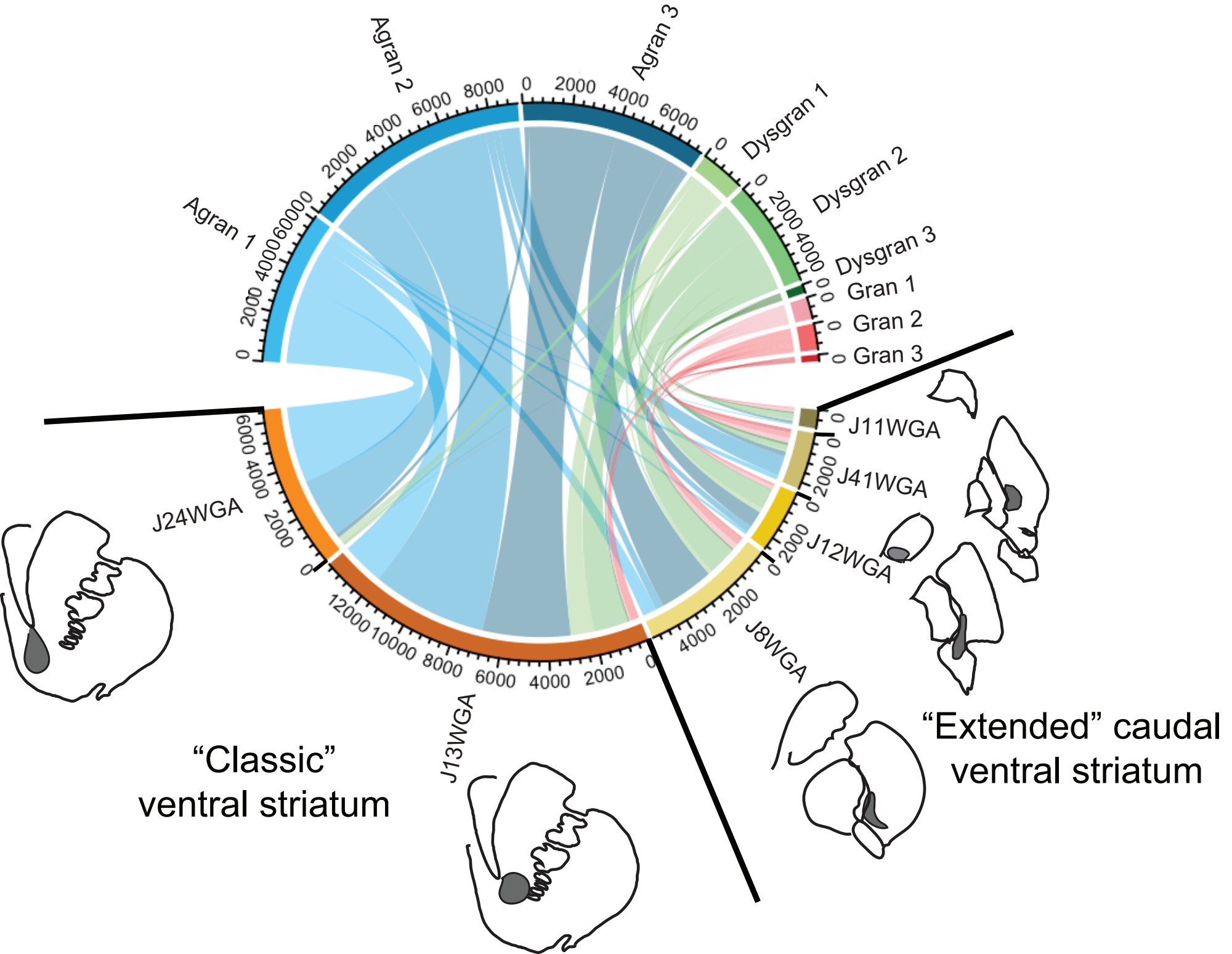
Agran 1
Agran 2
Agran 3
Dysgran 1
Dysgran 2
Dysgran 3
Gran 1
Gran 2
Gran 3
J11WGA
J41WGA
J12WGA
J8WGA
J13WGA
J24WGA
"Classic" ventral striatum
"Extended" caudal ventral striatum

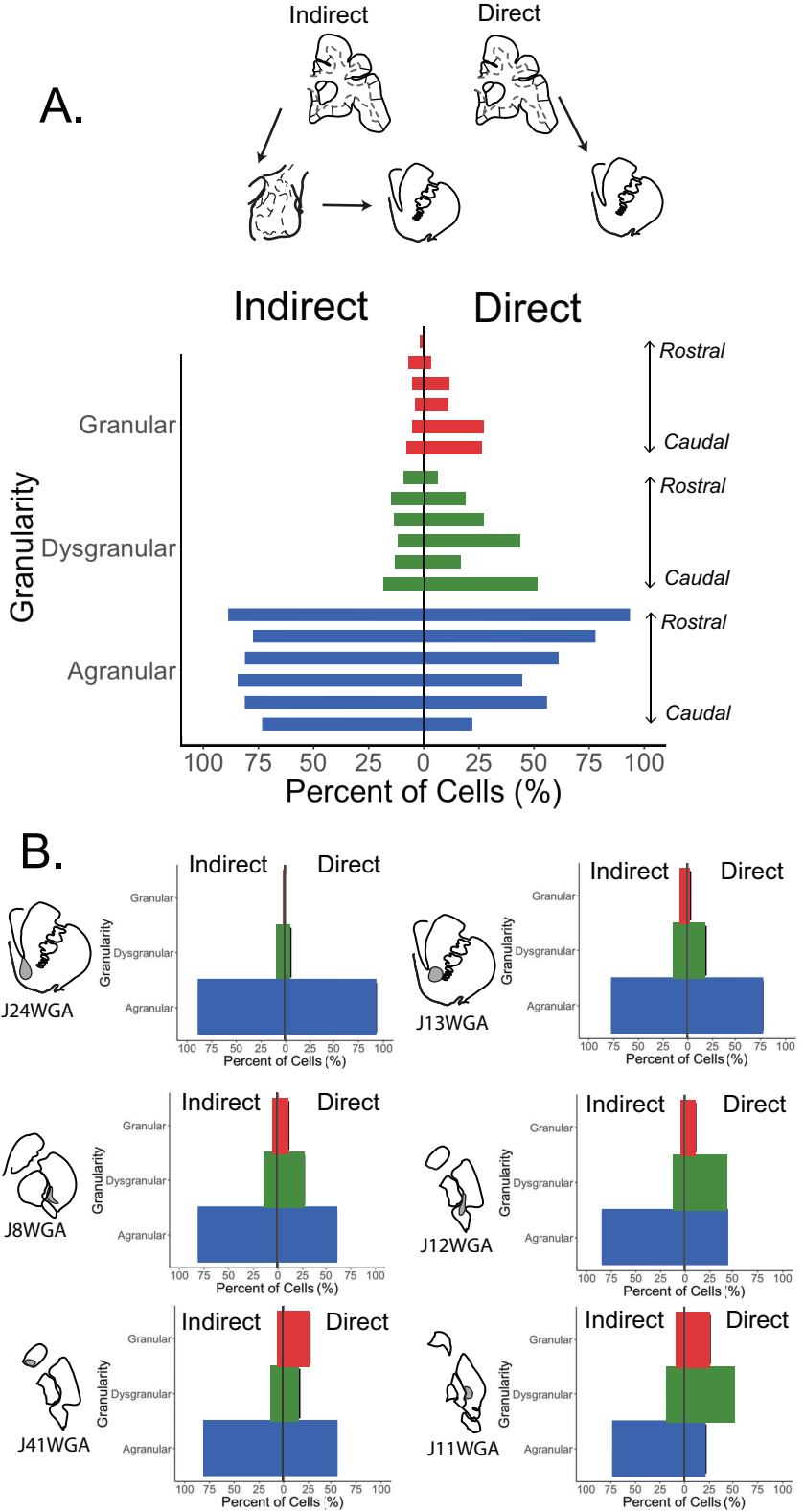
A.
Indirect
Direct
Indirect
Direct
Granularity
Granular
Dysgranular
Agranular
Rostral
Caudal
Rostral
Caudal
Rostral
Caudal
100 75 50 25 0 25 50 75 100
Percent of Cells (%)
B.
J24WGA
J13WGA
J8WGA
J12WGA
J41WGA
J11WGA
Indirect
Direct
Granularity
Granular
Dysgranular
Agranular
100 75 50 25 0 25 50 75 100
Percent of Cells (%)

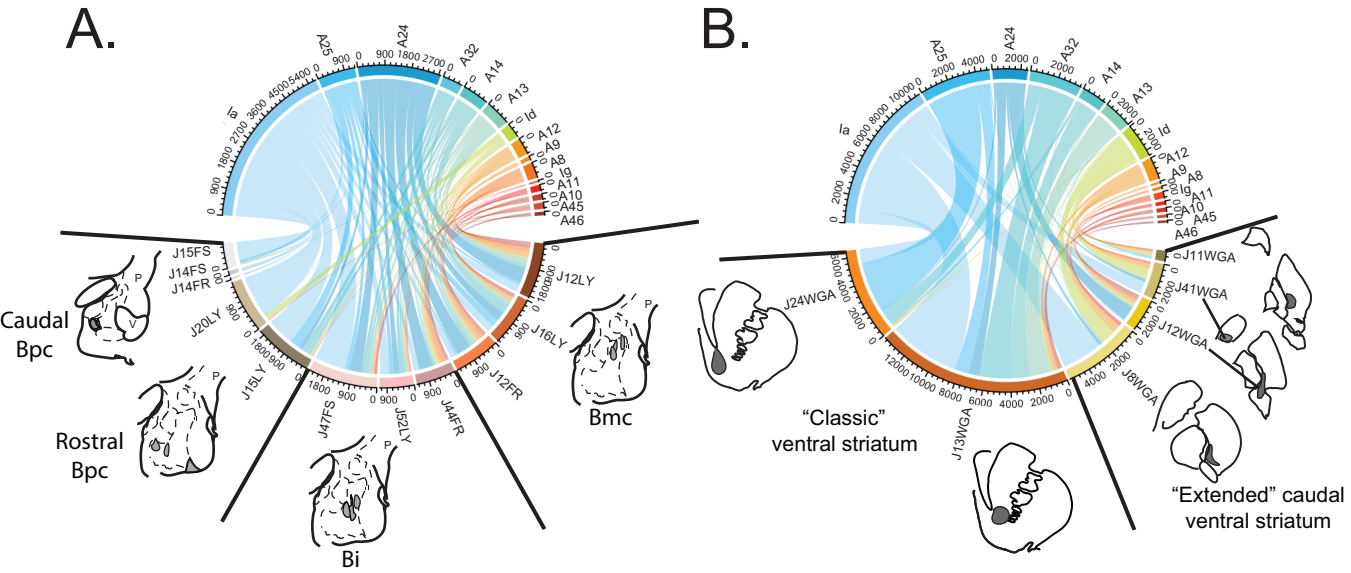
A.
B.
Caudal Bpc
Rostral Bpc
Bi
Bmc
"Classic" ventral striatum
"Extended" caudal ventral striatum
A25
A24
A32
A14
A13
Id
A12
A9
A8
Ig
A11
A10
A45
A46
J15FS
J14FS
J14FR
J20LY
J15LY
J47FS
J52LY
J44FR
J12FR
J16LY
J12LY
J24WGA
J13WGA
J8WGA
J12WGA
J41WGA
J11WGA
Ia

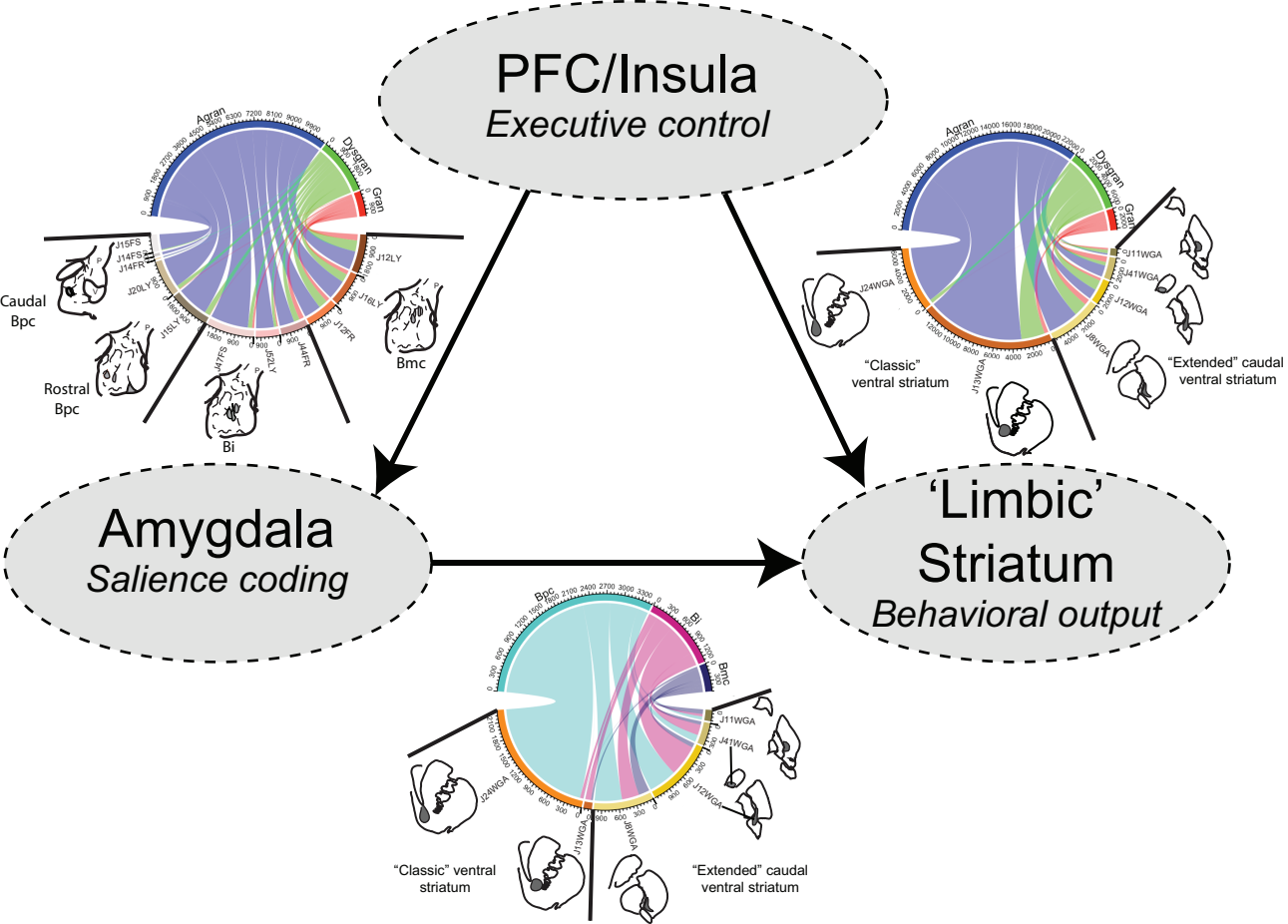
PFC/Insula
Executive control
Amygdala
Salience coding
'Limbic' Striatum
Behavioral output
Agran
Dysgran
Gran
J15FS
J14FS
J14FR
J20LY
J15LY
J47FS
J52LY
J46FR
J12PR
J16LY
J12LY
Caudal Bpc
Rostral Bpc
Bi
Bmc
J11WGA
J41WGA
J12WGA
J28WGA
J13WGA
J24WGA
"Classic" ventral striatum
"Extended" caudal ventral striatum
Bpc
Bi
Bmc